© 2020. Published by The Company of Biologists Ltd | Development (2020) 147, dev189472. doi:10.1242/dev.189472

STEM CELLS AND REGENERATION

RESEARCH ARTICLE

Evidence of two types of balance between stem cell mitosis and enterocyte nucleus growth in the *Drosophila* midgut

Vasilia Tamamouna*, Myrofora Panagi*, Andria Theophanous, Maria Demosthenous, Maria Michail, Markella Papadopoulou, Savvas Teloni, Chrysoula Pitsouli‡ and Yiorgos Apidianakis‡

ABSTRACT

Systemic and stem cell niche-emanating cytokines and growth factors can promote regeneration, through mitosis. High mitosis, however, predisposes for all types of cancer and, thus, a trade-off exists between regeneration capacity and tissue homeostasis. Here, we study the role of tissue-intrinsic regenerative signaling in stem cell mitosis of adult *Drosophila* midgut of different genetic backgrounds. We provide evidence of two naturally occurring types of balance between mitosis and enterocyte nucleus growth: one based mostly on stem cell mitosis producing new cells and the other based mostly on the degree of young enterocyte nucleus size increase. Mitosis promotes intestinal host defense to infection, but predisposes for dysplasia in the form of stem cell-like clusters. Enterocyte nucleus growth also promotes host defense, without the drawback of promoting dysplasia. Through quantitative genetics, we identified *eiger* as an autocrine and paracrine inducer of stem cell mitosis. *eiger* expression in immature epithelial cells tilts the balance towards mitosis and dysplasia via a positive-feedback loop of highly mitotic stem cells sustaining more small nucleus enterocytes, which in turn supply more Eiger.

KEY WORDS: Regenerative inflammation, Stem cells, Cancer predisposition

INTRODUCTION

Although the inflammatory microenvironment predisposes for tumor initiation and progression, the mechanisms that induce stem cells to become tumorigenic remain unclear. Known germline mutations account for a small percentage of cancers, whereas most cancers develop with age as a result of spontaneous somatic mutations propelled by inflammation (Hanahan and Weinberg, 2011). Chronic inflammation of the colonic mucosa provides the basis for colon cancer development and is accompanied by high mitosis and DNA damage (Balkwill and Mantovani, 2001; Lasry et al., 2016). Inflammatory signal transducer and activator of transcription protein (STAT) signaling and reactive oxygen species can directly drive regeneration and mutation (Karin and Clevers, 2016; Panayidou and Apidianakis, 2013; Taniguchi et al., 2015). Tissue-intrinsic mitosis level per se is a key factor correlating with carcinogenesis in humans (Tomasetti and Vogelstein, 2015; Tomasetti et al., 2017). Similarly, proliferative activity in the aging *Drosophila* midgut accompanies dysplasia, but also affects longevity, with maximal lifespan occurring when intestinal proliferation is reduced, but not completely inhibited (Biteau et al., 2010). The genetic factors controlling progenitor cell proliferation, and thus cancer predisposition, are mainly studied qualitatively, without accounting for the effects of inter-individual genetic differences and environmental influences on tissue-intrinsic mitosis (Wu et al., 2016).

The *Drosophila* midgut, like its mammalian counterpart, is frequently challenged by a plethora of abiotic and biotic stresses, which can damage the intestinal epithelial barrier, leading to pathogenesis. Accordingly, various homeostatic signaling mechanisms operate to tightly regulate epithelial cell turnover and shedding of damaged epithelial cells (Buchon et al., 2013; Karin and Clevers, 2016; Peterson and Artis, 2014). The *Drosophila* midgut is maintained by pluripotent intestinal stem cells (ISCs) that self-renew and give rise to transient enteroblasts (EBs), which terminally differentiate into polyploid enterocytes (ECs) (Micchelli and Perrimon, 2006; Ohlstein and Spradling, 2006). ISCs also give rise to pre-enteroendocrine cells (pre-EEs), the EE progenitors (Zeng and Hou, 2015). Signaling pathway ligands, such as Delta (Dl), Unpaired 3 (Upd3), Vein (Vn), *Drosophila* insulin-like peptides 3 and 6 (Dilp3 and 6) and Eiger (Egr) control ISC proliferation and/or EB differentiation (Apidianakis and Rahme, 2011; Kux and Pitsouli, 2014; Doupé et al., 2018), but mitosis can be diverted towards dysplasia as a result of the deregulation of the signaling pathways induced by such ligands (Apidianakis et al., 2009). For example, Notch pathway loss of function results in loss of EB differentiation and the accumulation of stem cell tumors (Micchelli and Perrimon, 2006; Siudeja et al., 2015). The epidermal growth factor receptor (EGFR) and Janus kinase (JAK)/STAT pathways promote ISC proliferation and their over-activation induces tumorigenesis. Similarly, the insulin and c-Jun N-terminal kinase (JNK) pathways are linked to ISC proliferation and dysplasia during aging (Amcheslavsky et al., 2009; Apidianakis et al., 2009; Biteau et al., 2008; Buchon et al., 2010; Jiang et al., 2009; Xiang et al., 2017). Adult midgut dysplasia in *Drosophila* has been characterized by the widespread, irreversible and progressive loss of proper cell differentiation, resulting in the accumulation of groups of ISC-like and EE cells (Apidianakis et al., 2009; Biteau et al., 2008; Resende et al., 2018); this is in contrast to the rare ISC-like/EE large tumors caused by spontaneous loss of heterozygosity of *Notch* in old flies (Siudeja et al., 2015).

A common property of differentiating *Drosophila* cells that need to cope with tissue development and homeostasis is endoreplicative cell growth. Endoreplication or endocycling is an evolutionarily conserved biological process whereby cells undergo repeated cycles of DNA replication without division, which usually leads to an increased nucleus size (Klusza and Deng, 2011; Shu et al., 2018; Tamori and Deng, 2014; Webster et al., 2009). A prerequisite for the

Department of Biological Sciences, University of Cyprus, 2109 Nicosia, Cyprus.
*These authors contributed equally to this work

‡Authors for correspondence (pitsouli@ucy.ac.cy; apidiana@ucy.ac.cy)

C.P., 0000-0003-4074-9684; Y.A., 0000-0002-7465-3560

Handling Editor: Cassandra Extavour
Received 11 December 2019; Accepted 17 April 2020

Development (2020) 147, dev189472. doi:10.1242/dev.189472

transition from mitotic cycles to endocycles is the inhibition of mitosis. Cyclin E (CycE) oscillations are known to control G to S phase transition in endoreplicating cells, but they also control G1 to S phase transition in mitotic cells of the larval wing discs in a context-dependent manner (Shu and Deng, 2017). CycE facilitates the expression of many S phase control genes (Duronio and O'Farrell, 1994; Shu et al., 2018) and its expression oscillates during the cell cycle, so that it accumulates during the S phase, but is absent during the G2 phase, to allow formation of the pre-replication complex required for the next round of DNA synthesis (Weiss et al., 1998). Thus, CycE expression and its cell cycle phase-dependent oscillation are necessary for cells to undergo either endoreplication or mitosis. CycE deregulation, however, may cause chromosomal instability and predisposition for bone, lung, liver, brain and intestinal cancer (Bortner and Rosenberg, 1997; Donnellan and Chetty, 1999; Malumbres and Barbacid, 2001).

Stem cell mitosis is tightly linked to cell differentiation in the *Drosophila* midgut. Upon midgut EC damage, the JAK/STAT and the EGFR signaling pathways are induced in the *Drosophila* ISCs to promote their mitosis, but also in EBs and/or young ECs to promote their differentiation (Jiang et al., 2009; Xiang et al., 2017). Endoreplication of young midgut ECs is an immediate regenerative response and initiates the first few hours after an oral infection, whereas ISC mitosis is induced later (Buchon et al., 2010; Xiang et al., 2017). The damaged adult epidermis and hindgut, which lack active stem cells, rely on the Hippo pathway to induce compensatory endoreplication in response to tissue damage (Losick et al., 2013). Moreover, the insulin/IGF-like pathway is needed for compensatory endoreplication in response to follicular epithelium cell loss (Tamori and Deng, 2013). The same pathway is necessary for midgut growth upon pupal eclosion and upon feeding on rich instead of poor media (Choi et al., 2011; O'Brien et al., 2011). Thus, both endoreplication and mitosis can be deployed to regenerate *Drosophila* epithelia. Yet, the balance between these key processes has been assessed only upon damage or stress, but not in terms of naturally occurring genetic variation.

Here, we investigate the coordination of DNA content regulation (which may include endoreplication), nucleus size and proliferation in the *Drosophila* midgut epithelium of 153 genetically disparate *Drosophila* Genetic Reference Panel (DGRP) lines and various transgenic genotypes, in the absence or presence of infection. In contrast to previous studies assessing tissue homeostasis and regeneration, we studied the role of genetic variation as a source of new information. We found that intestinal mitosis and EC nucleus size vary greatly as a function of the fly strain's genetic background and that certain tissue morphological characteristics may adapt to the high versus low mitosis status. Our quantitative genetics analysis demonstrated that, among the known signaling ligands supporting midgut stem cell mitosis, the secreted factor Egr plays a pivotal role in the counterbalance between mitosis and EC nucleus growth, which in turn impinges on host defense to infection and intestinal dysplasia. We provide evidence of two naturally occurring types of cell balance in the *Drosophila* midgut controlled by a positive feedback loop that involves the accumulation of ECs with a small nucleus that act as a source of paracrine mitogenic Egr.

RESULTS

Wild-type *Drosophila* strains exhibit extreme differences in ISC mitosis upon infection

Drosophila midgut stem cells are considered relatively inactive, but they are induced to divide at high levels by chemical stress or infection (Chatterjee and Ip, 2009). To genetically dissect the phenotypic variation of intestinal mitosis, we screened 153 sequenced wild-type (isogenized) DGRP strains (Mackay et al., 2012), measuring the number of mitotic cells per midgut after oral infection with the human opportunistic pathogen *Pseudomonas aeruginosa* (strain PA14) (Apidianakis et al., 2009). *Z*-score analysis of the mitotic index (Fig. 1A) underscored a great

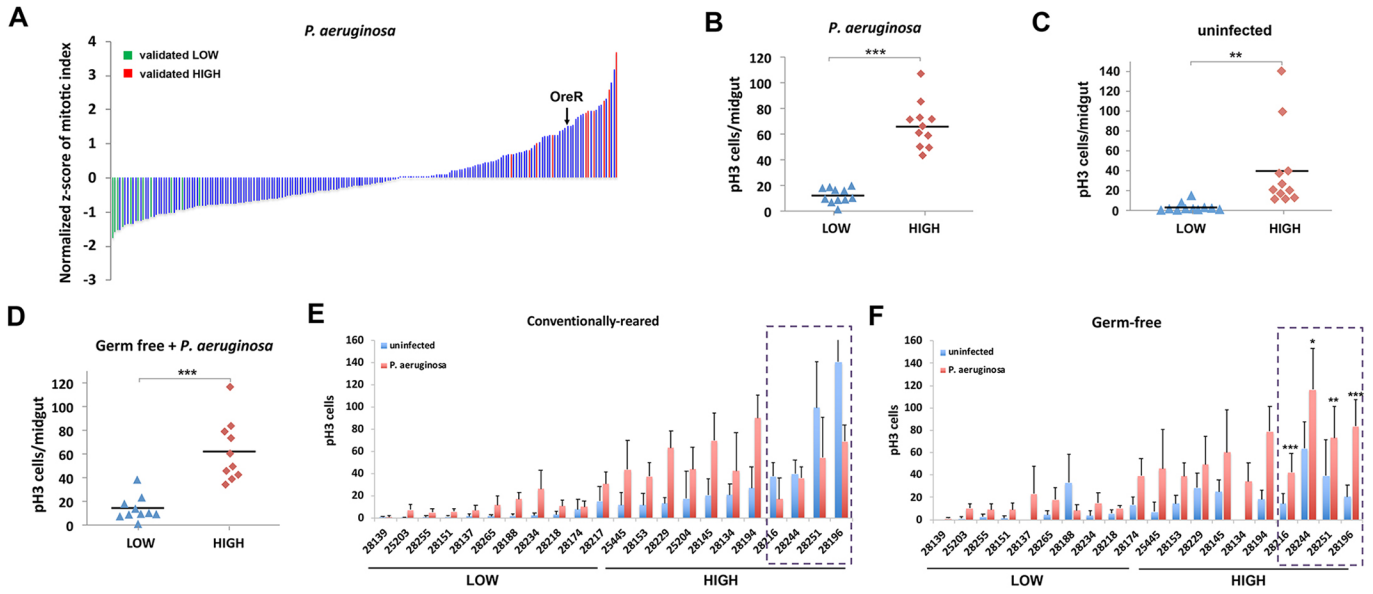

Fig. 1. Phenotypic variation among 153 DGRP lines pinpoints extreme high and low mitosis strains. (A) *Z*-score of the 153 DGRP lines exhibiting variation of >5 times the standard deviation. Green and red bars indicate validated low and high mitosis strains, respectively; arrow indicates the relative position of a common Oregon R strain. (B,C) Extreme low (28139, 25203, 28255, 28151, 28137, 28265, 28188, 28234, 28218, 18174, 28217) and high (25445, 28153, 28229, 25204, 28145, 28134, 28194, 28216, 28244, 28251, 28196) mitosis strains exhibit differential midgut mitosis (pH3 cells/midgut) with (B) or without (C) *P. aeruginosa* infection. (D) Germ-free low and high mitosis strains exhibit differential midgut mitosis upon infection. (E,F) Mitosis per midgut of conventionally reared (E) and germ-free (F) extreme strains with and without infection by *P. aeruginosa*. Rectangles indicate four strains lacking induction upon infection when conventionally reared (E), but not when grown as germ-free (F). Significance per two-sided *t*-test: *$P \leq 0.05$; **$P \leq 0.01$; ***$P \leq 0.001$.

Development (2020) 147, dev189472. doi:10.1242/dev.189472

variation in mitosis of up to five standard deviations of the mean among the strains tested. Upon repeated examination of the strains exhibiting extreme mitosis, we selected 22 with consistent phenotype (color highlighted in Fig. 1A): 11 of these exhibited high mitosis and 11 low mitosis (Fig. 1B). To pinpoint causal factors for the differences between the two groups of strains in terms of intestinal regeneration and dysplasia, we undertook a multiparametric approach, described in the following sections. We assessed bacteria associated with our flies, defense against infection, DNA content and size per nucleus, dysplasia and tissue-intrinsic regenerative signaling.

Strains exhibiting high mitosis upon infection are more resilient to infection and inherently prone to ISC mitosis without infection

To assess whether higher mitosis supports host defense against infection, we tested the survival of 11 strains exhibiting high mitosis and 11 with low mitosis upon *P. aeruginosa* infection in two different ways: each strain was either infected individually or infection was performed on a pooled population containing 5 flies from each of the 22 strains. To distinguish the strains with high and low mitotic activity in the pooled experiment, we introgressed *Dl-Gal4* and *UAS-srcGFP* in the genetic background of the 11 highly mitotic strains. Each day we used a fluorescent stereoscope to monitor the GFP-positive and GFP-negative flies that were infected and still alive. In both sets of experiments, we noticed that highly mitotic strains cope significantly better with lethal oral infection (Fig. S1A,B). Furthermore, the two extreme groups of strains contained comparable numbers of pathogenic bacteria upon infection (Fig. S1C). Thus, highly mitotic strains have better resilience to *P. aeruginosa* infection because they tolerate the pathogenic bacteria better without reducing them (Ferrandon, 2013; Schneider and Ayres, 2008).

Although intestinal microbiota and pathogenic bacteria can induce mitosis by damaging the epithelium directly or indirectly (Chatterjee and Ip, 2009; Lee et al., 2013), midgut mitosis in the highly mitotic strains was significantly higher even in the absence of infection (Fig. 1C), as well as in germ-free flies (Fig. 1D). Interestingly, microbiota competed with *P. aeruginosa*-mediated induction of mitosis in four of the highly mitotic fly strains, because only germ-free flies of these strains responded to *P. aeruginosa* infection (Fig. 1E,F). These four strains were still classified as highly mitotic based on their overall performance upon infection, whereas microbiota did not mask the induction of mitosis upon infection in the rest of the strains (Fig. 1E,F). Therefore, the strains selected as highly mitotic upon infection are, on average, inherently prone to mitosis.

Strains with high and low mitotic activity respond similarly to infection with regards to midgut size and cell stress or exfoliation

To assess whether gut dimensions were affected by the differential level of mitosis in strains exhibiting high and low mitosis, we assessed differences in midgut size before and after infection. We noticed that, despite initial differences, the two groups of strains responded similarly to infection. We found that midguts of the highly mitotic strains were generally longer (Fig. S2A-C), but all tested strains retained their length upon infection (Fig. S2D,E). In addition, highly mitotic strains had wider posterior midguts (Fig. S2F,G). Nevertheless, both groups of strains responded similarly to infection by increasing their anterior and posterior midgut width to comparable levels (Fig. S2H,I). Thus, baseline differences in size rather than differential tissue growth upon infection distinguishes the highly mitotic strains from those with low mitotic activity.

To assess whether differences in mitosis upon infection were a result of differences in epithelial physiology, we used methylene blue for transient staining of the *Drosophila* midgut epithelium, allowing measurement of the decoloration rate for each fly strain (Fig. S3A-C). The blue stain was not uniformly absorbed by the epithelium, whereas the stained intestines lost their color within 5 days, which was much faster than the duration of a complete cycle of cell renewal (Ohlstein and Spradling, 2006). Using only prominently stained flies of each genotype, we noticed increased decoloration upon *P. aeruginosa* infection (Fig. S3D). Infection is known to stress and kill midgut ECs (Apidianakis et al., 2009), and thus destaining is indicative of stained cell exfoliation or cytoplasmic purging (Lee et al., 2016). However, we did not observe any differences in the decoloration rates of strains with high versus low mitotic activity upon infection (Fig. S3E,F). In agreement with this, *puckered* (*puc*), a downstream target of the JNK pathway that is predominantly induced in stressed or damaged ECs (Apidianakis et al., 2009), was similarly expressed in the two groups of strains (Fig. S3G, Table S1). We suggest that the level of epithelial stress or exfoliation upon infection might not clearly distinguish the two extreme groups of fly strains.

Strain to strain variation indicates an inverse correlation between ISC mitosis and EC nucleus growth

To address whether the strains with low mitotic activity exhibited increased nucleus growth in response to infection, we measured the maximum nucleus cross-section area of the EC nuclei in the anterior and posterior midgut of all 22 strains (Fig. 2A-E). To obtain EC-specific nucleus size measurements, we set a threshold of >20 μm^2 in the nucleus maximum cross-section area to exclude the diploid ISC, EB and EE populations (Fig. S4). We found that the ECs of strains with low mitotic activity had larger nuclei than highly mitotic strains, both in the uninfected anterior and posterior midguts, whereas infection increased the nucleus size more clearly in strains with low mitotic activity, indicating an inverse relationship between ISC mitosis and EC nucleus growth (Fig. 2A-E).

To assess whether the observed EC nucleus size changes reflected differences in endoreplication, we measured both the EC nucleus maximum cross-section area and the EC DNA content of all 22 strains from the same images (Fig. S5). We found the EC nucleus size to correlate strongly with the EC nucleus DNA content in the eight conditions tested: anterior and posterior midgut of strains with high or low mitotic activity, infected or uninfected (Fig. S5E,F). In the anterior midgut, both the nucleus size and the DNA content were significantly different between the two sets of strains, with or without infection (Fig. S5A,C). In the posterior midgut, both the nucleus size and the DNA content were significantly different between the two sets of strains without infection, but only their nucleus size differed significantly upon infection (Fig. S5B,D). Any inconsistency between nucleus size and DNA content might be because the two do not always change proportionally (Webster et al., 2009), or because, unlike the DNA content measurements, the nucleus maximum cross-section area measurements are not affected by small random variations in DAPI staining intensity (see Materials and Methods).

Furthermore, we assessed changes in the percentage of all diploid cells (progenitors and EEs) in the total number of cells, but found no difference between strains with high versus low mitotic activity in response to infection: diploid cells increased significantly in the strains with high (from 22.9 to 27.4%, n=30, P<0.05) and low (from 20.7 to 26.2%, n=30, P<0.05) mitosis in the anterior midgut, but not significantly in the posterior midgut for either of the two

Development (2020) 147, dev189472. doi:10.1242/dev.189472

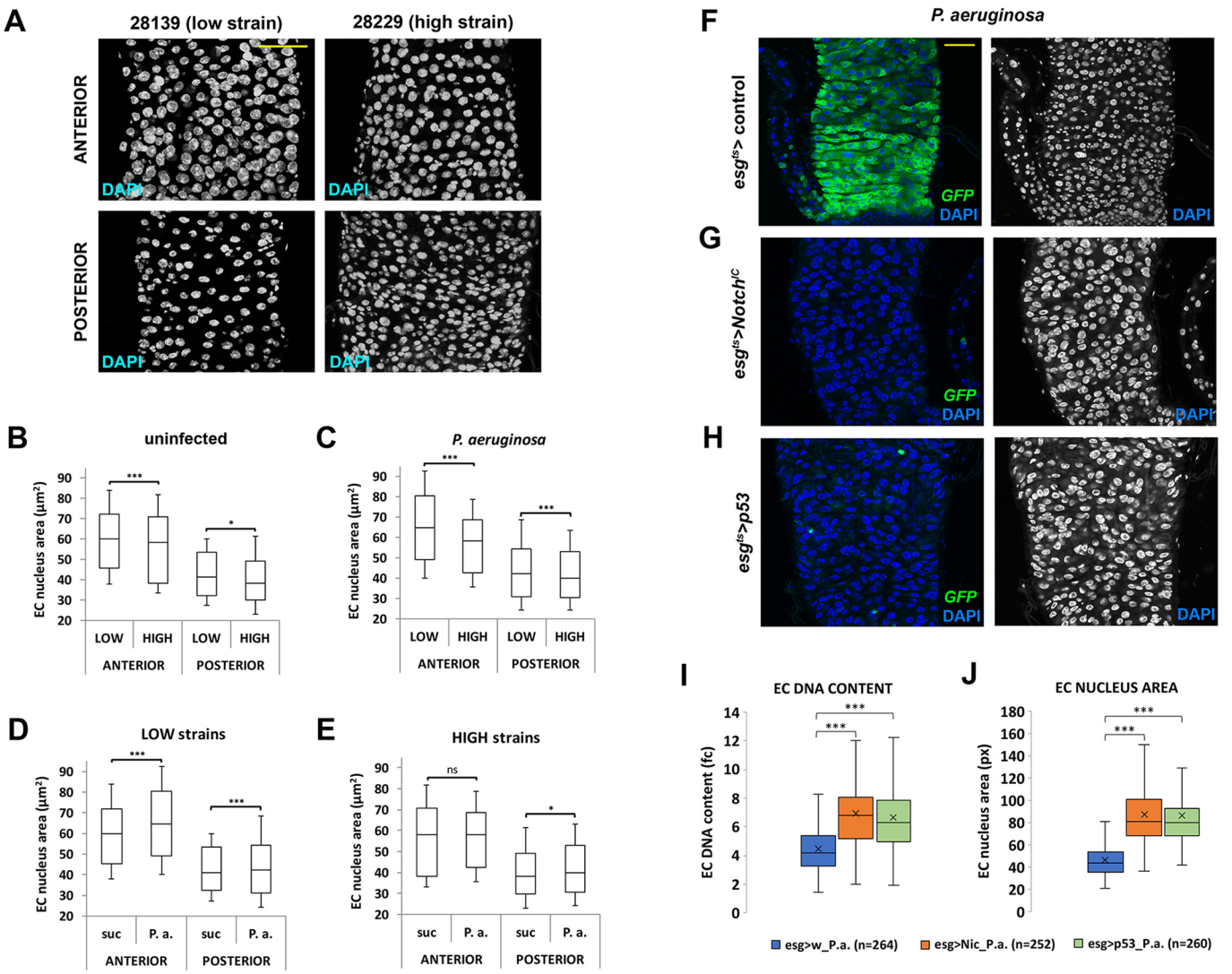

Fig. 2. Intestinal ISC mitosis inversely correlates with EC nucleus growth. (A) Representative images of DAPI-stained cell nuclei of anterior and posterior midguts of one low (28139) and one high (28229) mitosis strain without infection. (B-E) Quantification of anterior and posterior EC nucleus maximum cross-section area of midguts of the 11 low (anterior R2, *n*=1881; posterior R5, *n*=1553) and 11 high (anterior R2, *n*=1521; posterior R5, *n*=1332) mitosis strains without infection, and of the 11 low (anterior R2, *n*=2126; posterior R5, *n*=1611) and 11 high (anterior R2, *n*=1997; posterior R5, *n*=1228) mitosis strains with *P. aeruginosa* infection. (F-H) Representative images of DAPI-stained cell nuclei of infected posterior midguts expressing GFP in intestinal progenitors via *esg-Gal4*^{ts} (F), GFP plus *Notch*^{IC} that promotes ISC differentiation (G) or GFP plus *p53* that kills ISCs (H). (I,J) Quantification of EC DNA content relative to small midgut cells (I) and nucleus maximum cross-section area in pixels of midguts of the genotypes described in F-H (J). Significance per two-sided *t*-test: ns, $P>0.05$; *$P\leq0.05$; ***$P\leq0.001$. Scale bars: 50 µm.

groups (from 25.3 to 27.9% and from 22.3 to 23.3% for high and low mitosis strains, respectively). Thus, both groups of strains respond to infection by increasing their width and diploid cells at comparable levels (Fig. S2H,I), but low mitosis strains increase their EC nucleus size more prominently as a compensatory mechanism for tissue growth (Fig. 2B-E).

To further explore the possible proliferation-endoreplication interplay, we genetically ablated the adult midgut ISC population by expressing specifically in progenitor cells (*esg*$^{+}$) a constitutively active form of the Notch receptor composed of only its intracellular domain (Notch^{IC}) or the pro-apoptotic protein p53 (Fig. 2F-H). Although infection expanded the progenitor pool in wild-type flies (Fig. 2F), *esg*+ progenitors were barely evident upon *Notch*^{IC} or *p53* overexpression in adults (Fig. 2G,H). The absence of progenitors in both cases resulted in substantially enlarged nuclei compared with the control sample (Fig. 2F-H). Quantification was performed by measuring the DNA content and nucleus area. The two methods produced comparable results (Fig. 2I,J), demonstrating that in the absence of mitotic cells, infected ECs multiply their DNA and increase their nucleus size as a compensatory mechanism to meet tissue homeostasis demands.

Cell autonomous and non-cell autonomous control of ISC mitosis and EC nucleus growth by CycE

CycE is a key regulator of cell cycle S phase in both endoreplicative and mitotic embryonic *Drosophila* cells (Knoblich et al., 1994). Accordingly, we set out to assess whether genetic manipulation of *CycE* expression in mitotic ISCs and differentiating EBs affects their functions. *CycE* overexpression in ISCs increased mitotic activity by ∼twofold in the infected and uninfected midguts, but reduced the nucleus size of ECs in the anterior and the posterior uninfected midguts (Fig. 3A,B). Upon infection, *CycE* expression

Development (2020) 147, dev189472. doi:10.1242/dev.189472

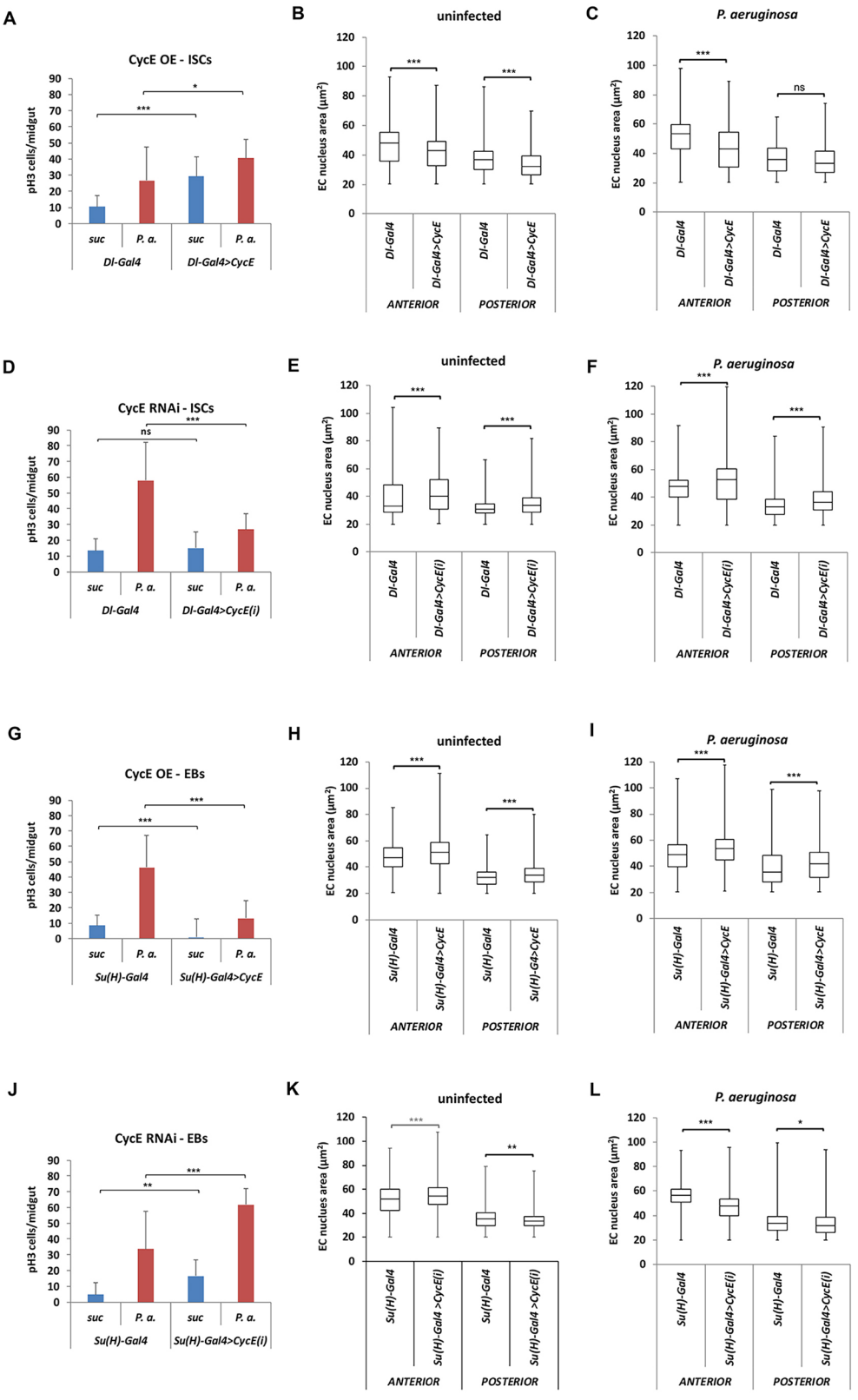

Fig. 3. Reciprocal antagonism between ISC mitosis and EC nucleus growth. (A-C) Midgut mitosis (A) and EC nucleus size in anterior R2 and posterior R5 midgut regions without (B) and with (C) *P. aeruginosa* infection upon *CycE* overexpression in ISCs using *Dl-Gal4* (uninfected, *n*=451, 530 nuclei in *Dl-Gal4* control R2 and R5, and *n*=509, 588 nuclei in *Dl-Gal4>CycE* R2 and R5, respectively; infected, *n*=619, 454 nuclei in *Dl-Gal4* control R2 and R5, and *n*=432, 352 nuclei in *Dl-Gal4>CycE* R2 and R5, respectively). (D-F) Midgut mitosis (D) and EC nucleus size without (E) and with (F) *P. aeruginosa* infection upon *CycE* RNAi knockdown in ISCs using *Dl-Gal4* (uninfected, *n*=635, 727 nuclei in *Dl-Gal4* control R2 and R5, and *n*=510, 695 nuclei in *Dl-Gal4>CycE*^{RNAi} R2 and R5, respectively; infected, *n*=637, 620 nuclei in *Dl-Gal4* control R2 and R5, and *n*=497, 554 nuclei in *Dl-Gal4>CycE*^{RNAi} R2 and R5, respectively). (G-I) Midgut mitosis (G) and EC nucleus size without (H) and with *P. aeruginosa* (I) infection upon *CycE* overexpression in EBs using *Su(H)-Gal4 Gal4* (uninfected, *n*=341, 477 nuclei in *Dl-Gal4* control R2 and R5, and *n*=389, 578 nuclei in *Dl-Gal4>CycE* R2 and R5, respectively; infected, *n*=559, 411 nuclei in *Dl-Gal4* control R2 and R5, and *n*=502, 435 nuclei in *Dl-Gal4>CycE* R2 and R5, respectively). (J-L) Midgut mitosis (J) and EC nucleus size without (K) and with *P. aeruginosa* (L) infection upon *CycE* RNAi knockdown in EBs using *Su(H)-Gal4* (uninfected, *n*=344, 405 nuclei in *Dl-Gal4* control R2 and R5, and *n*=446, 384 nuclei in *Dl-Gal4>CycE*^{RNAi} R2 and R5, respectively; infected, *n*=565, 512 nuclei in *Dl-Gal4* control R2 and R5, and *n*=565, 531 nuclei in *Dl-Gal4>CycE*^{RNAi} R2 and R5, respectively). Significance per two-sided *t*-test: ns, $P>0.05$; *$P\leq0.05$; **$P\leq0.01$; ***$P\leq0.001$.

in ISCs also reduced EC nucleus size in the anterior, but only tentatively so in the posterior (Fig. 3C). Conversely, downregulation of *CycE* specifically in the ISCs decreased mitosis by ∼twofold upon infection and increased the nucleus size of ECs in the anterior and the posterior midgut before and after infection (Fig. 3D-F).

On the other hand, *CycE* overexpression specifically in the EBs reduced intestinal mitosis by ≥fourfold upon infection, but increased EC nucleus size in the anterior and posterior midgut in the presence or absence of infection (Fig. 3G-I). Conversely, downregulation of *CycE* in EBs increased mitosis by ∼twofold

Development (2020) 147, dev189472. doi:10.1242/dev.189472

upon infection and decreased EC nucleus size, with notable exception of the uninfected anterior midgut (Fig. 3J-L). We conclude that CycE promotes mitosis cell autonomously in the ISCs and suppresses EC nucleus size non-cell autonomously; vice versa, CycE promotes EC nucleus size cell autonomously in EBs and suppresses mitosis non-autonomously.

Analysis of FlyGut-seq data (Buchon et al., 2013) showed a higher expression ratio of CycE in EBs versus ISCs in the anterior midgut (2.88 in the R1 region and 1.56 in R2), compared with the posterior midgut (0.7 in R4 and 0.44 in R5) (Fig. S6A). This might explain the bigger EC nuclei of the anterior compared with posterior midgut (Figs 2 and 3) and the higher mitosis noted in the posterior compared with the anterior midgut (Fig. S6B,C). Taken together, these results suggest that the relatively higher CycE in the anterior EBs increases their nucleus size, whereas the relatively higher CycE in the posterior ISCs boosts their proliferation.

Increase in EC nucleus size by CycE improves host defense to infection

To assess the impact of EC nucleus size on host defense against infection, we measured fly survival after feeding with *P. aeruginosa*, when *CycE* was overexpressed or downregulated in EBs. *CycE* overexpression in EBs increased EC nucleus size (Fig. 3H,I) and fly survival to infection (Fig. S7A,A′) at the expense of ISC mitosis (Fig. 3G). *CycE* downregulation in EBs, did not inhibit EC nucleus size uniformly (Fig. 3J-L) and did not improve fly survival consistently (Fig. S7A,A′). We conclude that the cell autonomous increase in the nucleus size of young ECs through CycE promotes host defense to infection.

CycE downregulation in ISCs, which inhibits mitosis (Fig. 3D), also reduces fly survival (Fig. S7B,C), despite the increase in EC nucleus size (Fig. 3E,F). This indicates that the increase in EC nucleus size cannot fully compensate for the reduction in mitosis and phenocopies the increased survival rates of the highly mitotic strains that exhibited smaller EC nuclei (Fig. S1A,B).

Interestingly, *CycE* overexpression in ISCs, which promoted mitosis at the expense of EC nucleus size in the anterior midgut (Fig. 3A-C), consistently reduced fly survival (Fig. S7B,C). We suggest that the cell autonomous induction of mitosis in ISCs by CycE leads to improper EC differentiation or function. This is supported by data showing that *CycE* overexpression in ISCs increased dysplastic cell cluster formation, whereas *CycE* downregulation in ISCs decreased dysplasia (Fig. 4I). We conclude that both ISC mitosis and the increase in nucleus size of young ECs may protect the *Drosophila* midgut from infection and that improper EC differentiation through excessive mitosis may compromise fly resilience to intestinal pathogens.

Highly mitotic strains are prone to dysplastic cell cluster formation

We next sought to assess whether highly mitotic strains are prone to midgut dysplasia, which normally occurs during aging or in genetically predisposed flies upon infection (Apidianakis et al., 2009; Biteau et al., 2008; Marianes and Spradling, 2013; Siudeja et al., 2015). Infection of young flies and chemical inhibition of Notch (via the γ-secretase inhibitor DAPT) resulted in more dysplastic cell clusters, i.e. groups of five or more ISC-like cells or EEs (Fig. 4A), in the highly mitotic strains (Fig. 4B,C). Even untreated flies of the highly mitotic strains developed more dysplastic cell clusters at a young age (Fig. 4D,E) in agreement with their higher expression of the ISC marker *Dl* (Guo and Ohlstein, 2015) (Fig. 5A). Moreover, the mitosis level correlated with dysplastic cell cluster incidence within an independent set of four additional genotypes (Fig. S8A-D). Also, increasing or decreasing ISC mitosis directly through *CycE* overexpression or *CycE* downregulation in ISCs, respectively (Fig. 3A,D), altered dysplastic cell cluster incidence upon infection and Notch pathway inhibition according to the level of mitosis (Fig. 4I-J). Additionally, 30- and 42-day-old flies of the highly mitotic strains developed more dysplastic cell clusters upon aging (Fig. 4F-H,M-O) and the posterior midgut, which exhibits increased overall mitosis compared with the anterior (Fig. S6B,C), was more inflicted by dysplastic cell clusters (Fig. 4K,L,P,Q). Thus, ISC mitosis is a key factor in promoting intestinal dysplasia in the form of dysplastic ISC-like/EE cell clusters, which accumulate rapidly in young chemically treated and infected flies or progressively in flies upon aging.

egr expression is strongly associated with ISC mitosis

To explain mitotic variation at the molecular level, we combined two approaches to pinpoint relevant genes: (a) candidate gene expression assessment via comparative RT-qPCR of the 11 highly mitotic strains versus the 11 strains with low mitosis, and (b) a genome-wide association study (GWAS) assessing mitotic variation among the 153 DGRP strains.

Out of 26 candidate genes related to *Drosophila* immunity or regeneration, we identified the *Dl*, *upd3*, *vn* and *egr* ligands as exhibiting tentatively increased expression in the highly mitotic strains without infection (Fig. 5A-D; Table S1). *Dl*, *upd3* and *vn* are known stem cell signaling regulators, whereas *egr* has been more recently linked to stem cell mitosis (Buchon et al., 2010; Doupé et al., 2018; Guo and Ohlstein, 2015; Jiang et al., 2009). Our GWAS analysis identified 95 variants, including single nucleotide polymorphisms (SNPs) and small insertions-deletions (INDELs), associated with midgut mitosis, corresponding to 39 protein-coding genes (Table S2). These genes could affect mitosis either locally in the midgut or systemically. Ubiquitous downregulation of eight of these genes was lethal to the flies, but downregulation of seven other genes plus *egr* reproducibly affected ISC mitosis. RNAi-mediated downregulation of *CG8475*, *proPO45*, *CG4991* and *egr* reduced mitosis, whereas downregulation of *sda*, *Snx6*, *Fign* and *Snoo* increased mitosis (Fig. 5E). To identify potential cross-regulation between *Dl*, *upd3*, *vn* and *egr* and the newly identified GWAS genes, we correlated the expression of each of these ligands with the mitosis level of flies compromised in expression of the seven mitosis-related GWAS genes plus *egr* (Fig. 5F-I). We found that *egr* expression was the only one to positively and significantly correlate with the level of mitosis in these flies (Fig. 5I; P=0.0071). Thus, *egr* expression has a key role in ISC mitosis.

Tissue-intrinsic Egr acts as an accelerator of mitosis and dysplasia at the expense of EC nucleus growth

To identify the tissues and cell types in which *egr* is needed for ISC mitosis, we altered its expression systemically in the fat body and hemocytes, tissues previously shown to express *egr* and affect organismal metabolism and inflammation (Agrawal et al., 2016; Mabery and Schneider, 2010; Parisi et al., 2014) (Fig. S9). Although *egr* was induced in the fat body upon intestinal infection (Fig. S9A,B), we did not observe any impact of systemic *egr* expression on ISC mitosis upon infection (Fig. S9C,D). To the contrary, we noticed a tissue-intrinsic role for *egr* by manipulating its expression levels in all midgut epithelial cells (ISCs plus EBs plus ECs) (Fig. 6A). Downregulation of *egr* in all midgut epithelial cells eliminated infection-induced ISC mitosis, whereas *egr* overexpression was sufficient to increase mitosis in the absence of

Development (2020) 147, dev189472. doi:10.1242/dev.189472

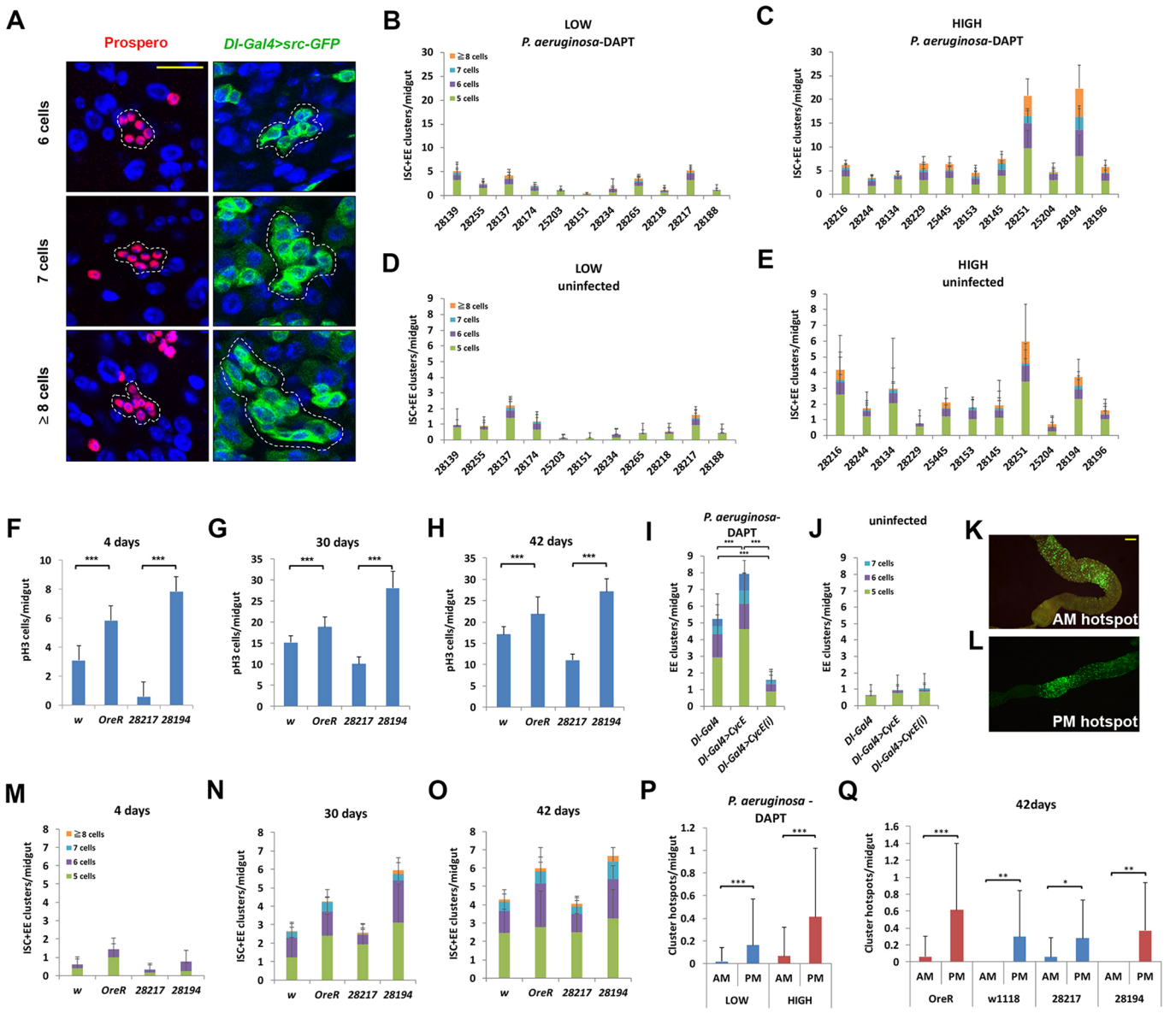

Fig. 4. ISC and EE dysplastic cell cluster enumeration in the midgut upon aging and in chemically treated and infected flies. (A) Prospero (red) and *Dl-Gal4 UAS-srcGFP* (green) cell clusters of 6, 7 and ≥8 cells. (B-E) The 11 low versus 11 high mitosis strains differ in cluster numbers per female midgut in the presence of infection plus DAPT (*y*-axis set to 30 in B,C), and in uninfected conditions (*y*-axis set to 9 in D,E). (F-H,M-O) Differences in mitotic cells (F-H) and ISC+EE clusters (M-O) per female midgut during aging of four strains of different genetic backgrounds bearing the *Dl-Gal4 UAS-srcGFP* transgenes. (I,J) *CycE* and *CycE*^{RNAi} expression in ISCs with *Dl-Gal4* in the presence (I) and absence (J) of infection plus DAPT. (K,L) Hotspots of *Dl-Gal4 UAS-srcGFP*-positive cell clusters in the anterior (K) and posterior (L) midgut. (P,Q) Enumeration of cluster hotspots in the anterior and posterior midgut in DAPT/infected (P) and 42-day old flies (Q). Significance per two-sided *t*-test (B,E,F-H) and chi-square test (I,J,M-O,P,Q): **P*≤0.05; ***P*≤0.01; ****P*≤0.001. Scale bars: 25 µm (A), 100 µm (K,L).

infection (Fig. 6A). Overexpression of *egr* specifically in ISCs or EBs or ISCs+EBs significantly induced ISC mitosis upon infection, whereas progenitor-specific downregulation of *egr* consistently reduced mitosis, exhibiting its maximum impact when *egr* was downregulated simultaneously in both ISCs and EBs (Fig. 6B-D). The effect of *egr* in ECs was less clear and not consistent between the uninfected and the infected states, indicating that *egr* plays more than one role in these cells (Fig. 6E).

In terms of stem cell numbers, overexpression of *egr* in ISCs using *ISC*^{ts}*-Gal4 UAS-GFP* increased the GFP-positive cells at baseline and upon infection (Fig. 6F,G). Moreover, *egr* overexpression via *ISC*^{ts}*-Gal4 UAS-GFP* induced dysplastic cell clusters both in the presence and the absence of infection (Fig. 6H,I) and promoted spontaneous tumor formation upon aging (Fig. 6J). Thus, intrinsic expression of *egr* in ISCs and other epithelial cells increases their proliferation and predisposition for tumorigenesis.

Using *egr-Gal4 UAS-dsRed* flies, we noticed *egr* expression in the ISCs and EBs along the whole midgut, but also in ECs in two low mitosis zones (tA1 and R5) (Fig. 6K-O). *egr* rarely co-localized with Prospero (1.5% of *egr*+ cells upon infection, *n*=530, and 1.8% without infection, *n*=550), which labels the EEs and their precursors (Guo and Ohlstein, 2015; Zeng and Hou, 2015). In addition, we used an Egr-GFP protein trap line (Sarov et al., 2016) and found that Egr was localized in the cytoplasm of intestinal progenitors and ECs, but not EEs (Fig. S10). Interestingly, we noticed that mitosis spikes in the A2 and P3 regions of the midgut, the exact same

Development (2020) 147, dev189472. doi:10.1242/dev.189472

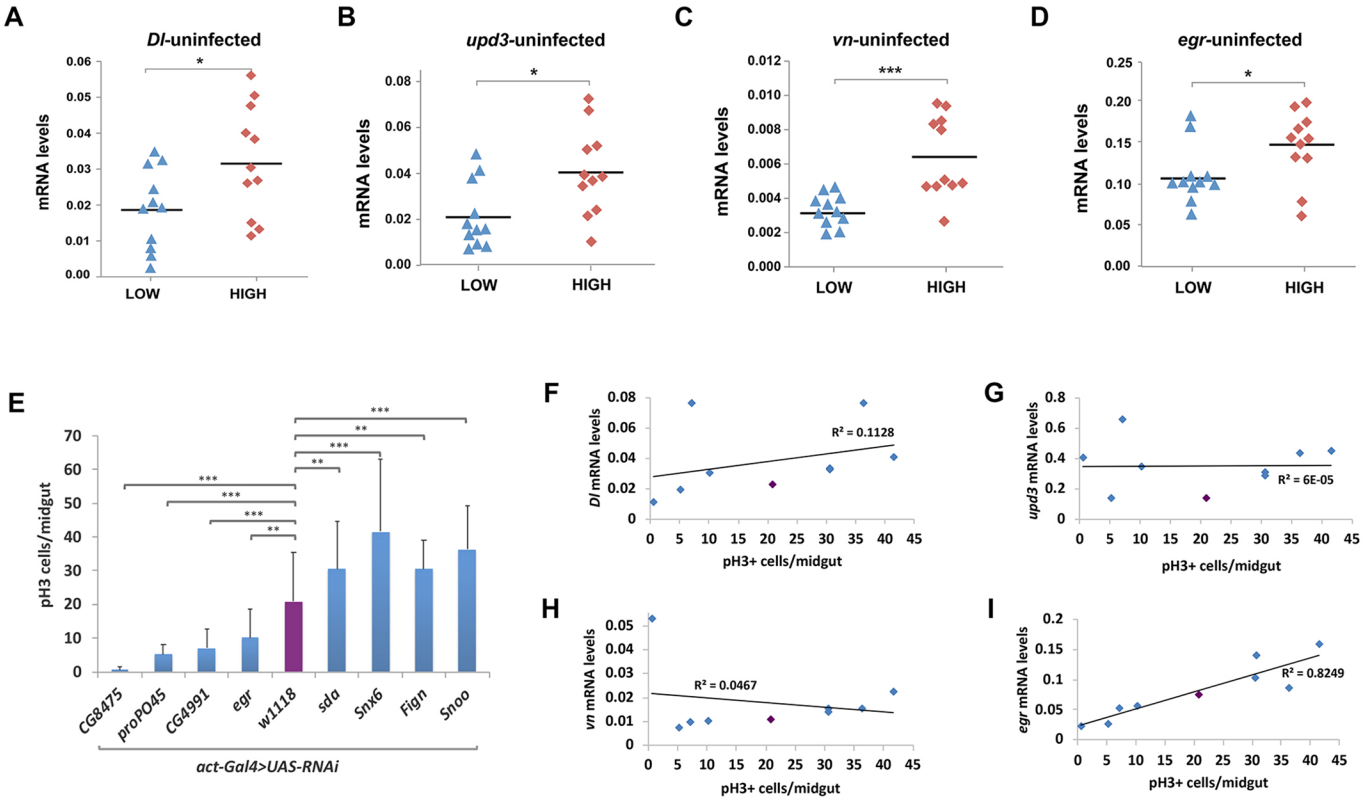

Fig. 5. Tentatively higher expression of regenerative inflammation genes in the highly mitotic strains. (A-D) The 11 low versus 11 high mitosis strains exhibit different expression levels of *Dl* (A), *upd3* (B), *vn* (C) and *egr* (D) in uninfected baseline conditions. (E) Midgut mitosis of *P. aeruginosa*-infected flies with ubiquitous knockdown (via *act-Gal4-UAS-RNAi*) of *egr* and seven polymorphism-associated genes. (F-I) Gene expression to midgut mitosis correlation for *Dl* (F), *upd3* (G), *vn* (H) and (I) *egr* in control and knocked-down genotypes shown in E. Two-sided *t*-test: *$P \leq 0.05$; **$P \leq 0.01$; ***$P \leq 0.001$.

regions with the highest progenitor (ISCs+EBs) to EC ratio of *egr* expression (Fig. 6P,Q). Of note, *egr* expression was not induced upon infection in the midgut (Fig. S11A; Table S1). Furthermore, Ras signaling induction in ISCs, which is necessary and sufficient for regeneration upon infection (Jiang et al., 2011), did not induce *egr* (Fig. S11B). We conclude that *egr* expression is inherently controlled in the midgut progenitors through baseline signals rather than those induced upon infection.

To assess the role of *egr* in the interplay between midgut mitosis and EC nucleus growth, we downregulated and overexpressed *egr* in ISCs without and upon infection. *egr* RNAi led to an increase in EC nucleus size in the anterior and the posterior midgut without and upon infection (Fig. 7A,B). In contrast, *egr* overexpression led to a decrease in EC nucleus size in the posterior midgut without and upon infection (Fig. 7A,B), whereas mitosis was increased upon infection in the same midgut region (Fig. 7C,D). Thus, *egr* expression in ISCs may directly promote mitosis in ISCs and dysplasia at the expense of EC nucleus growth.

Finally, we found that EB-specific *Notch* RNAi reduced EB differentiation, promoting EB cluster formation (Fig. 7E), which was accompanied by the heightened expression of *egr* in the epithelium (Fig. 7F). This indicates that accumulation of progenitor cells producing mitogenic Egr may sustain a high level of ISC mitosis. Considering also that additional ligands expressed in the midgut progenitors contribute to ISC mitosis (Chen et al., 2016; Patel et al., 2015; Zhai et al., 2015), we propose that a positive feedback loop operates in the *Drosophila* midgut whereby highly mitotic stem cells sustain more differentiating cells of the EC lineage, which in turn supply more Egr (Fig. 7G).

DISCUSSION

Drosophila and mammals have evolved two mechanisms for maintaining tissue integrity upon injury: compensatory cell proliferation and compensatory growth of differentiated cells (Huh et al., 2004; Tamori and Deng, 2014). The *Drosophila* midgut responds to injury by deploying both mechanisms at the same time; that is, ISC mitosis is followed by EC growth to replenish the damaged ECs with new fully differentiated ones (Xiang et al., 2017). We also found a coordinated induction of mitosis and EC nucleus growth in our study; yet, this coordination was not the same for all genotypes. Some genotypes exhibited relatively high mitosis but low EC nucleus growth, and others exhibited relatively low mitosis but high EC nucleus growth. Our study provides evidence that differentiating ECs increase their nucleus size, and may undergo more endoreplication cycles to sustain intestinal integrity and dimensions, when mitosis is limited. We showed that the level of mitosis per fly midgut differed significantly from strain to strain, even without infection. Nevertheless, during infection both high and low mitosis strains increased their anterior and posterior midgut width to comparable levels. The increase in midgut width upon infection was accompanied by an increase in EC nucleus size in the anterior and posterior midgut, which was more prominent in the strains with low mitotic activity. Although this increase in nucleus size allowed the low mitosis strains to cope with injury, these strains were more susceptible to bacterial infection. Thus, the increase in nucleus size of young ECs may provide a mechanism of tissue recovery from EC damage that is less effective than mitosis-driven cell renewal.

Development (2020) 147, dev189472. doi:10.1242/dev.189472

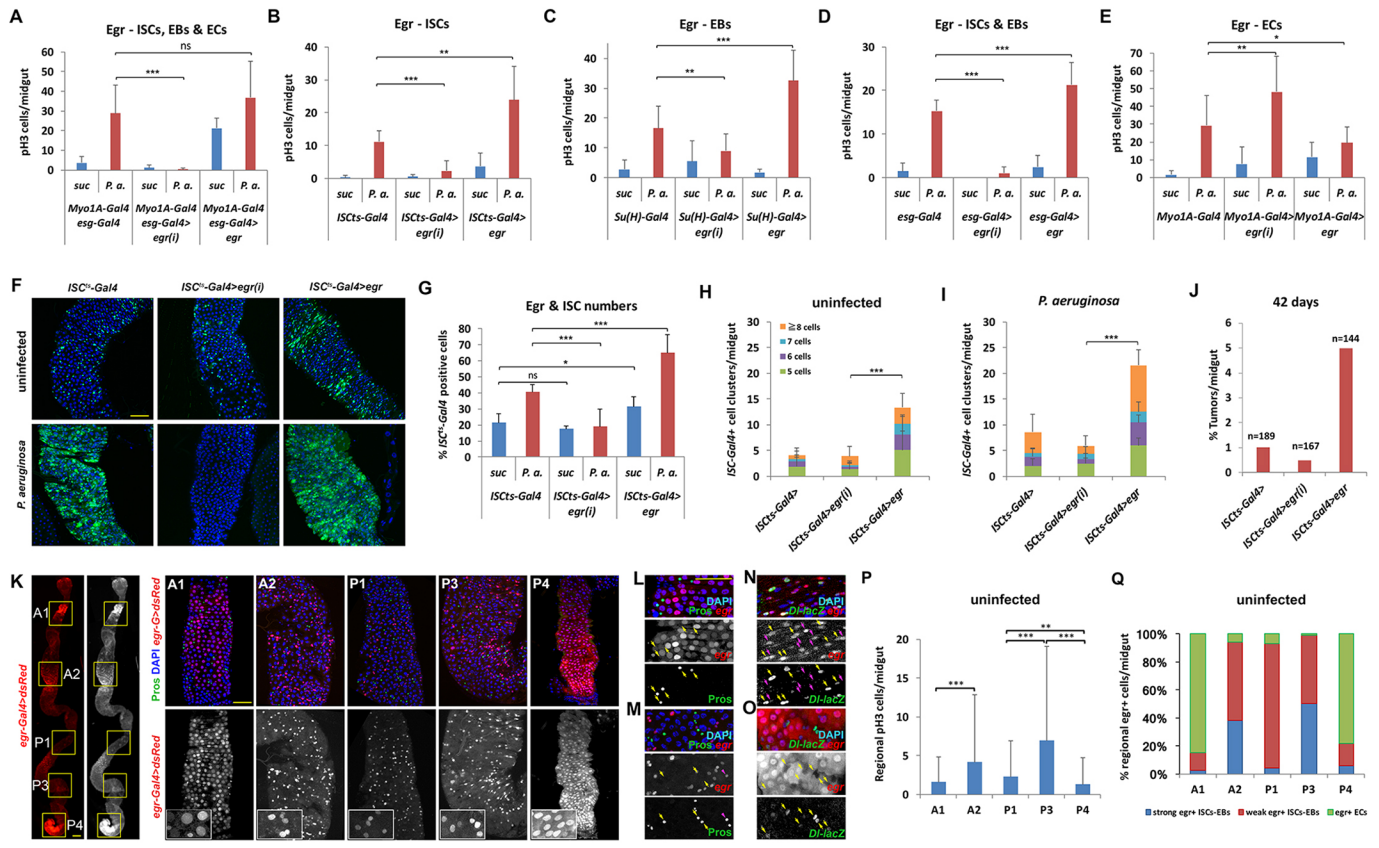

Fig. 6. *egr* expression varies along the midgut and its expression in progenitors promotes mitosis and dysplasia. (A-E) Midgut mitosis upon *egr* overexpression and *egr* RNAi in the absence (suc) and presence of infection (P.a.) in ISCs+EBs+ECs (A), ISCs only (B), EBs only (C), ISCs+EBs (D) and ECs only (E). (F,G) Representative images (F) and image-based quantification (G) of ISC^{ts}-GFP-positive cells in *egr* RNAi and *egr* overexpression flies exhibiting decreased and increased ISC numbers, respectively, with and without infection. (H-J) *egr* RNAi and *egr* overexpression in ISCs affects dysplastic ISC-like and EE cell clusters without (H) and with (I) infection, as well as age-associated tumor incidence (J). (K) Expression pattern along the midgut of *egr-Gal4 UAS-dsRed* flies exhibiting prominent EC expression in A1(R1) and P4(R5) and strong progenitor expression in A2(R2) and P3(R4c). Anti-Prospero staining (green) highlights the EEs. The first two panels are composites of single midguts with images of all regions stitched together manually. (L,M) Prospero (yellow arrows in single channel images) and *egr* (red) co-localize only rarely (purple arrowhead) in A1(R1). (N,O) Prominent, but not exclusive, co-localization in P1(R4a) of *Dl-lacZ* (green, yellow arrows in single channel images) with *egr* (red, purple arrows in single channel images). (P) Mitotic cells per A1(R1), A2(R2), P1(R4a), P3(R4c) and P4(R5) region in uninfected midguts. (Q) Percentage of strongly and weakly *egr*-expressing progenitors, and *egr*-expressing ECs per A1, A2, P1, P3 and R5 region in uninfected midguts. Significance per two-sided *t*-test (A-E,G,P) and chi-square test (H-J): ns, $P>0.05$; *$P\leq0.05$; **$P\leq0.01$; ***$P\leq0.001$. Scale bars: 50 µm.

To assess whether the interplay between ISC proliferation and EC nucleus growth was causal, we genetically manipulated these processes cell autonomously. We found that ISC elimination (via activated *Notch* or *p53* expression) yielded a prominent increase in EC nucleus size, whereas even a mild reduction in ISC mitosis (via *CycE* downregulation) yielded a mild, but significant, increase in EC nucleus size. Moreover, *CycE* overexpression in ISCs induced mitosis mildly, resulting in a mild, but significant, non-cell autonomous decrease in EC nucleus size. Importantly, there was reciprocity in this cause and effect, because a mild induction of EC nucleus growth via *CycE* overexpression in EBs reduced ISC mitosis mildly. Yet, this reciprocity was not physiologically equal, because high ISC mitosis increased the midgut susceptibility to dysplasia, whereas high EC nucleus size did not. Both ISC mitosis and the increase in EC nucleus size were necessary for optimal host defense to infection, but excessive mitosis predisposed for dysplasia, which compromised host defense. In this respect, EC nucleus size increase may benefit the host as a primary response to injury or increase in nutrient availability in a timely manner, even if mitosis is eventually needed to restore tissue integrity. In agreement with our study, injury has been shown to deploy endoreplication as a faster or necessary way to achieve homeostasis in *Drosophila* (Buchon et al., 2010; Choi et al., 2011; Losick et al., 2013) and mice (Denchi et al., 2006) and as an energy-saving process for producing the necessary cell surface membrane in plants (Kondorosi et al., 2000).

Based on our data stemming from naturally occurring genetic variation, we propose the existence of two contrasting types of homeostatic or regenerative balance between cell renewal and cell growth with regards to host defense: a type-I balance based primarily on ISC mitosis to support defense to infection that also makes flies more susceptible to dysplasia, which, in turn, impedes host defense; and a type-II balance based mostly on EC nucleus growth (possibly through EB endoreplication), which boosts host defense without the drawback of dysplasia (Fig. 7H). High tissue mitosis is inextricably linked to high cancer incidence (Tomasetti and Vogelstein, 2015; Tomasetti et al., 2017), indicating that a delicate balance is optimal for organismal health, whereby relatively low mitosis benefits homeostasis and moderately high mitosis is beneficial during infection. Low mitosis might also be beneficial against tumorigenesis, because (a) mitotic cells are prone to replication errors in the DNA, which can be propagated

Development (2020) 147, dev189472. doi:10.1242/dev.189472

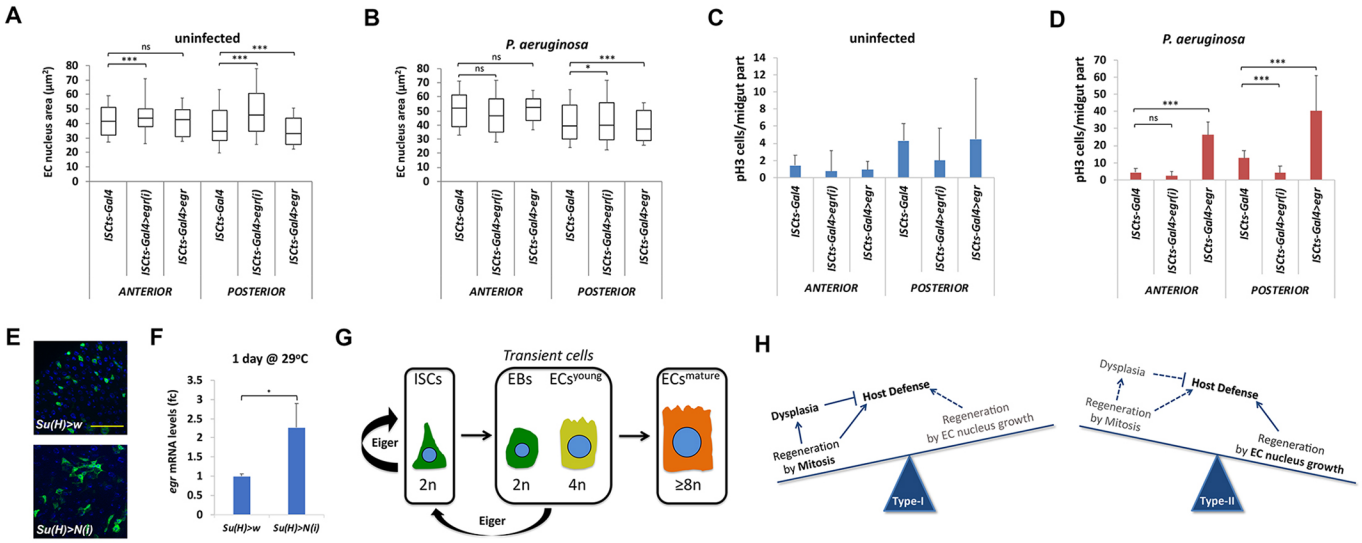

Fig. 7. *egr* tilts the ISC mitosis-EC nucleus growth balance in the midgut towards mitosis via a positive feedback loop that sustains progenitor cells. (A-D) *egr* RNAi and *egr* overexpression in ISCs affect EC nucleus size non-autonomously in the posterior midgut without (A) and with (B) *P. aeruginosa* infection (uninfected, *n*=534, 550, 426 nuclei in ISC^{ts}-*Gal4* control, ISC^{ts}>egr^{RNAi}, ISC^{ts}>*egr*, respectively, in midgut region R2, and *n*=823, 850, 750 nuclei in ISC^{ts}-*Gal4* control, *ISCts*>egr^{RNAi}, ISC^{ts}>*egr*, respectively, in midgut region R5; infected, *n*=390, 689, 546 nuclei in ISC^{ts}-*Gal4* control, ISC^{ts}>egr^{RNAi}, ISC^{ts}>*egr*, respectively, in midgut region R2, and *n*=744, 956, 670 nuclei in ISC^{ts}-*Gal4* control, *ISCts*>egr^{RNAi}, ISC^{ts}>*egr*, respectively, in midgut region R5). The effects are inversely correlated with mitosis without (C) and with (D) *P. aeruginosa* infection. (E,F) Representative images of GFP-labeled EBs (E) and relative *egr* expression (F) of *Su(H)-Gal4 UAS-GFP* $tub80^{ts}$ fly midguts inducing *Notch* RNAi versus control 1 day post transfer to the permissive temperature (*n*=12). Error bars represent s.e.m. (G) Model depicting the type I versus type II balance between mitosis and EC nucleus growth and their impact on host physiology. (H) Model depicting a positive feedback loop sustained by Egr emanating from EBs and young ECs. Two-sided *t*-test: ns, $P>0.05$; *$P\leq0.05$; **$P\leq0.01$; ***$P\leq0.001$. Scale bar: 50 µm

indefinitely if in active stem cells, and (b) highly endoreplicated cells, although still DNA error prone, contain multiple gene copies, some of which are still wild type, that may buffer the effect of tumor suppressor gene mutations.

Drosophila strains exhibiting excessive mitosis upon infection tended to express regenerative genes at higher levels. We pinpoint four key signaling pathway ligands in controlling the high level of mitosis: the homeostasis ISC marker Dl, the stress-induced cytokine Upd3 emanating from ECs, the visceral muscle-emanating growth factor Vn and the cytokine Egr, which is expressed in most ISCs and EBs (Doupé et al., 2018). The latter was the least studied and we found that it plays a key role in ISC mitosis. Mild autocrine *egr* expression in ISCs may not suffice to induce mitosis in the absence of a secondary stimulus, but stronger or paracrine *egr* expression does. In agreement with this, *egr* expression in ISCs in the context of intestinal infection clearly induced ISC mitosis. Thus, Egr is a secreted mitogen that, similarly to Upds and other ligands, can be released both systemically and locally at the midgut epithelium (Agrawal et al., 2016; Chakrabarti et al., 2016). Regenerative factors can be induced upon infection and cell stress via STAT signaling in flies and mice (Jiang et al., 2009; Taniguchi et al., 2015), and our work provides a new example of a mitogen that is constantly and tissue-intrinsically expressed in the intestine. Midgut *egr* expression is not induced upon infection or upon the activation of mitosis-inducing Ras signaling in ISCs (Jiang et al., 2011). Instead, *egr* is steadily expressed in progenitors and ECs (Dutta et al., 2015), and we show that loss of EB differentiation increases *egr* expression in the midgut. We suggest that highly mitotic stem cells produce at any given time more immature progeny, namely EBs and young ECs, which in turn express and supply more Egr to neighboring ISCs (Fig. 7G). Such a positive feedback loop can be reinforced by additional mitogenic ligands expressed in the midgut progenitors (Chen et al., 2016; Patel et al., 2015; Zhai et al., 2015). Moreover, given the impact of the microenvironment in controlling ISC mitosis (Choi et al., 2011; Maeda et al., 2008; Patel et al., 2015), we suggest that a regenerative signaling through Egr and other mitogens and cell growth factors may be regulated pharmacologically or through diet and probiotics to optimize regenerative capacity and tissue resilience to infection, while decreasing predisposition for dysplasia.

MATERIALS AND METHODS

Fly stocks

All stocks were maintained at 25°C on a 12:12 h light:dark cycle on fly food containing yeast, cornmeal, sugar and agar supplemented with Tegasept and propionic acid. The 153 inbred strains of the DGRP collection were obtained from the Bloomington *Drosophila* Stock Center (BDSC). The 48 *UAS-RNAi* lines of genes selected through GWAS analysis (Table S2) were obtained from the Vienna *Drosophila* Resource Center (VDRC). Of these, 40 produced viable progeny when crossed to *w; Actin5C-Gal4 UAS-srcGFP/CyO* (originating from BDSC #25374 and BDSC #5432). The rest were crossed to *w; myo1A-Gal4 UAS-EGFP/CyO* (gift from Bruce Edgar, University of Utah, USA). All UAS-RNAi lines were isogenized by backcrossing to our laboratory control strain w^{1118} for more than six generations.

The following Gal4 lines were used for tissue and cell-type specific expression: for EC expression, *tub-Gal80*^{ts}*/FM7; myo1A-Gal4 UAS-EGFP/CyO* (Apidianakis et al., 2009); for progenitor expression, *w; esg-Gal4 UAS-GFP tub-Gal80*^{ts} (Apidianakis et al., 2009); for EB expression, *w; Su(H)-Gal4 UAS-CD8GFP tub-Gal80*^{ts20}*/CyO* (Zeng et al., 2010); for ISC expression, *w; UAS-src-GFP/CyO; Dl-Gal4 tub-Gal80*^{ts}*/TM6C* (Zeng et al., 2010) and *esg-Gal4 UAS-GFP; Su(H)-Gal80 tub-Gal80*^{ts} (Zeng and Hou, 2015); for visceral muscle expression, *w; how*^{24B}*-Gal4 UAS-EGFP/TM3* (originating from BDSC #1767) and *w; dmef2-Gal4 UAS-dsRed/TM3* (Ranganayakulu et al., 1996) were combined with *tub-Gal80*^{ts} on the X; for EC and progenitor expression, *w; esg-Gal4 UAS-GFP myo1A-Gal4* (recombined on the second chromosome); for fat body expression, *w; yolk-Gal4* (gift from Norbert Perrimon, Harvard Medical School, USA); and for fat body and hemocyte expression, *w; cg-Gal4*

Development (2020) 147, dev189472. doi:10.1242/dev.189472

(BDSC #7011), *w; UAS-egr^{RNAi}* (VDRC# 108814 KK), *w; UAS-egr^{strong}* (Andersen et al., 2015), *w; UAS-CycE^{RNAi}* (VDRC# 110204 KK), *w; UAS-CycE* (BDSC #4781), *UAS-Notch^{IC5}* (Go et al., 1998), *UAS-p53* (BDSC #8420). *w^{1118}* was used as a control for all UAS transgenic lines, in which all lines were isogenized (Evangelou et al., 2019), and Oregon R as a typical wild-type strain. GAL4-UAS crosses were reared at 18°C and adult flies were transferred to 29°C for 5 days to induce the transgenes before experiments. To assess the expression pattern of *egr* along the *Drosophila* midgut, *egr-Gal4/CyO*, *Act-GFP* (Mabery and Schneider, 2010) flies were crossed to *UAS-dsRed/TM3* (BDSC #6282) and *ry^{506} Dl-lacZ^{05151}/TM3* (BDSC #11651) (Ranganayakulu et al., 1996). Crosses were reared at 25°C and adult flies were transferred to 29°C for 2 days of aging before the experiment. The FlyFos line (VDRC #318615) was used as an Egr-GFP protein trap (Sarov et al., 2016).

Oral infection assays

Oral infection assays were performed as previously described (Apidianakis et al., 2009). Briefly, a single colony from the *P. aeruginosa* strain PA14 was grown at 37°C to OD_{600nm}=3, corresponding to 5×10^9 bacteria/ml. Female mature flies of the desired genotype were starved for 5 h and added in groups of 10 per fly vial containing a cotton ball at the bottom impregnated with 5 ml of 0.5 ml PA14 OD_{600nm}=3, 1 ml 20% sucrose and 3.5 ml dH_2O. For the uninfected control, 5 ml of 1 ml sucrose 20% and 4 ml dH_2O was used. Flies were incubated for 48 h at 25°C (for the DGRP screening) or 29°C (for all experiments utilizing the Gal4-UAS system, unless otherwise noted).

Survival assays

For individual *Drosophila* line testing, triplicates of ten 3- to 5-day-old female flies for each extreme DGRP line were infected with the *P. aeruginosa* strain PA14, as described above. The numbers of dead and alive flies were recorded daily.

For the pooled strain survival assay, 5 female flies from each of the 11 highly mitotic DGRP strains containing the isogenized *UAS-srcGFP; Dl-Gal4* transgenes were mixed into a fly bottle with 5 female flies from each of the 11 low mitosis DGRP lines. The cohorts were infected in fly bottles containing four cotton balls at the bottom impregnated with 20 ml of 2 ml PA14 culture (OD_{600nm}=3), 4 ml 20% sucrose and 14 ml dH_2O. Flies were incubated at 25°C. The number of dead and alive flies expressing GFP (high mitosis) and not expressing GFP (low mitosis) was recorded daily with the use of the fluorescent Leica M165 FC stereoscope.

Dissections and immunohistochemistry

Dissections and immunohistochemistry were performed as previously described (Apidianakis et al., 2009). Briefly, 15 midguts were dissected each time from each fly genotype in 1× PBS and fixed for 30 min with 4% formaldehyde (FA) at room temperature. Three quick rinses were performed with 1× PBS. Blocking was with 1× PBS, 0.2% Triton-X, 0.5% BSA for 20 min. Primary antibodies were rabbit anti-phosphohistone H3 (pH3; 1:4000; 06-570, Millipore), mouse anti-Prospero (1:100; MR1A, DSHB), mouse anti-β-gal (1:500; Z378A, Promega), chicken anti-GFP (1:1000; A10262, Invitrogen) and rabbit anti-GFP (1:3000; A6455, Invitrogen) incubated overnight in the dark at 4°C. Midguts were washed three times for 10 min in 1× PBS containing 0.2% Triton-X. Secondary antibodies against mouse, rabbit conjugated to Alexa 555 (A31572, Invitrogen) or chicken conjugated to Alexa Fluor 488 (A11039, Invitrogen) were used at 1:1000. Samples were incubated in secondary antibody solution including DAPI (1:3000 of 10 mg/ml stock; Sigma) for 2 h at room temperature in the dark, with mild shaking. Midguts were washed three times, mounted on glass microscope slides in 20 µl of Vectashield (Vector), covered with glass coverslips and sealed with nail polish.

Image acquisition and analysis

Stacks of optical sections were acquired using the Leica TCS SP2 DMIRE2 confocal microscope. Images to be compared were taken using the exact same settings. The numbers of pH3 cells were counted under the fluorescent microscope (Zeiss Axioscope A.1) at 20× magnification along the whole midgut. For regional assessment of A1(R1), A2(R2), P1(R4a), P3(R4c) and P4(R5), a standard frame of 300×350 µm per region per midgut was covered.

Midgut sizes (length and width) were assessed from bright-field pictures acquired with a fluorescent Leica M165 FC stereomicroscope and their width and length analyzed using ImageJ (https://imagej.nih.gov/ij/). Clicking on the Analyze, Set Scale option, the length of the picture was set at 2048 pixels, corresponding to 2.07 mm. Using the segmented line option, a line was drawn manually, starting from the cardia and ending just before the hindgut proliferating zone (HPZ). For the width measurement, straight lines indicating the width of posterior A1 and anterior R5 were manually drawn vertically to the gut length. The length of the lines was measured, and thereby the gut dimensions, by clicking on the Analyze, Measure option.

The nucleus maximum cross-section area (Figs 2B-E, 3 and 7) was measured following analysis of non-saturated confocal images using ImageJ. Confocal images of anterior (R2) and posterior (R5) midguts were captured at 40× magnification, zoom 1× and 1024×1024 format and produced as a maximum projection of 10-15 sections serial imaging. By clicking Analyze, Set Scale option, the distance in pixels was set at 1024 and known distance at 375 µm, according to confocal photo properties. Multichanneled images were subjected to the Split Channel option to isolate the blue signal (DAPI staining). The images were subsequently converted into grey by selecting the Image option, Lookup Tables and Grey color option. Then, the adjustment of threshold was applied to produce 2 pixel intensities on the photo; black and white. A binary version of the images was generated and the type of measurement was specified to the Analyze particles option: show outlines. The infinity value was set to either 1 or 2, to exclude calculation of random speckles in the photo. Display Results, Clear Results, Summarize, Exclude Edges and Include Holes options were also selected. Measurements of area corresponding to each numbered nucleus were exported to Microsoft Excel to calculate the mean and median nucleus area values. Merged nuclei were excluded manually to improve the efficiency of calculations.

For DNA content measurements (Fig. 2I,J; Fig. S5), the same confocal images as above were utilized, but sum projections were assessed instead of max projections. Sum projections were used to measure the total DAPI fluorescence from individual nuclei using ImageJ in anterior and posterior images of the midguts. Specifically, each and every nucleus (excluding nuclei that overlapped) was selected manually using the circular selection tool of the software and, then, measurements for nucleus maximum cross-section area and integrated density were acquired. The data were exported and analyzed in Excel, so that the DAPI signal of each nucleus per midgut image was normalized to the average signal of small cells (progenitors and EEs). This was deemed necessary given the variability of the DAPI intensity between midguts. Then, the normalized data points of hundreds of cells arising from the same part (anterior or posterior) of at least three midguts were added and used to generate BoxPlots in Microsoft Excel. For these measurements, generation of binary images (a qualitative way to measure nucleus surface that does not account for signal intensity, used above for automated selection of individual nuclei) was not an option, because they would not be quantitative. As seen in the data of Xiang et al. (2017), no distinct ploidy was apparent. This could indicate that the endoreplication of midgut enterocytes is a very dynamic process, with many cells being in a transitory partially replicated state.

Statistical analysis

The *Z*-value of each strain was calculated by subtracting the average pH3 number of all 153 strains from the pH3 number of the strain and dividing the result by the standard deviation of the pH3 number of all 153 strains. It represents the number of standard deviations a particular DGRP line was found above or below the mean of all 153 lines.

We used the two-tailed Student's *t*-test to compare the means of two groups of values, namely, the pH3-positive numbers per midgut (n=30 midguts per genotype), the relative mRNA levels in high versus low mitosis strains (n=11 strains, 3 biological replicates for each), CFUs (n=10 strains, 3 biological replicates for each), midgut dimensions (n=11 strains, 10 midguts for each), decoloration (n=11 strains, 3 biological replicates for each) and the

Development (2020) 147, dev189472. doi:10.1242/dev.189472

nucleus area (n=11 strains, 3 midguts for each, >100 counts each). Data were assessed for normality of distribution with the mean value minimally deviating from the median. For sample size >200, the t-test is robust even for heavily skewed distributions (Fagerland and Sandvik, 2009).

Chi-square test was used to compare the number of total cell clusters of ≥5 cells per genotype between two genotypes, sampling the same number of midguts (n=30 midguts) and expecting the same number of clusters per genotype. For one degree of freedom, chi-square values were all >10.82, corresponding to significance P<0.01. Error bars represent s.d. Chi-square was also used to assess tumor incidence as being different among three genotypes (control, egr^{RNAi} and *egr* overexpression) exhibiting 2, 1 and 7 tumors per 189, 167 and 144 midguts, respectively. For two degrees of freedom, the chi-square was >13.81, corresponding to significance of P=0.001.

For fly survival and decoloration curve assessment, we applied the Kaplan–Meier method using the log-rank test (MedCalc statistical software).

Upon optimization, each experiment was replicated independently for a total of three biological replicates in addition to any technical replicates. Results are presented considering all replicates. Error bars throughout represent standard deviation of the mean (s.d.) except where noted. Significance is indicated by *P<0.05, **P<0.01, ***P<0.001; ns, not statistically significant.

RT-qPCR

For each of the 11 'high' versus 11 'low' extreme DGRP strains in both uninfected and infected conditions, the average of three biological replicates was used to assess the relative expression of regenerative inflammation genes (P-values are provided in Table S1). For the Ras^{V12} expression experiment, the average of three biological replicates (3 technical replicates for each) was used. RNA was extracted from 20 midguts per strain per condition per biological replicate using Qiazol (Qiagen). We used 800 ng of total RNA to synthesize the cDNA using the RQ1 RNase-Free DNase Kit (Promega) according to the manufacturer's protocol. Reverse transcription was performed using 145.4 ng of the total DNase-treated RNA using the TaKaRa Prime Script RT Master Mix Kit. qPCR amplification was performed using gene-specific primers with the following amplification program: 95°C for 30 s (initial denaturation), 40 cycles of 95°C for 10 s (denaturation), 60°C for 30 s (annealing, extension) and 65°C for 1 min (final extension). Primer sequences for each gene are shown in Table S3. Expression of the genes of interest was normalized to the expression levels of two reference genes, *rpl32* and *gapdh1*, using the $2^{-\Delta\Delta Ct}$ method. Data were analyzed using the Bio-Rad CFX Manager 3.1 program.

Dysplastic cell cluster enumeration

w; UAS-srcGFP; Dl-Gal4 flies were backcrossed to the 22 extreme DGRP lines for six generations by selecting GFP+ larvae in each generation to obtain the genetic background of the original DGRP line, while having GFP-marked ISCs. Flies of 5-7 days old from each strain were orally infected with the *P. aeruginosa* for 24 h at 25°C as described above and transferred into 50 ml falcon tubes bearing 12 1.2 mm holes on the lid (for access to food) and 32 0.5 mm holes on the tube surface (for aeration), using flame-heated 18 g×40 mm and 25 g×16 mm needles to pierce the tube lid and surface, respectively. A 23 mm Whatman disc (Sigma-Aldrich) impregnated with 270 µl of a solution composed of 1 mM DAPT (Sigma-Aldrich) dissolved in 30% yeast paste was placed on the outside of the tube lid and stabilized with parafilm. Flies were treated with DAPT for 4 days at 25°C and flipped every day into clean falcons with freshly prepared drug.

Methylene blue – EC coloration

Adult females of 5-7 days old were fed 0.5% methylene blue (Sigma) dissolved in 85% heat-killed yeast paste for 5 h at 25°C secondary to 5 h starvation. Flies were then subjected to either bacterial infection or 4% sucrose feeding for 2 days. Then, flies were fed 4% sucrose and recorded every day according to their color status (blue versus non-blue abdomen) until complete decoloration of their guts was observed.

Bacterial load

P. aeruginosa (PA14 strain) colony forming units (CFUs) per fly strain were determined following 2 days of infection at 25°C. Flies were externally sterilized by brief dipping into pure ethanol, dried and placed into 2 ml Eppendorf tubes containing 200 µl lysogeny broth (LB) and a stainless-steel bead of 5 mm diameter (Qiagen). Flies were homogenized using the TissueLyser II (Qiagen) at 50 Hz for 5 min. LB was then added into the tubes containing the tissue lysate to reach the volume of 1000 µl. Serial dilutions of the lysate obtained from three flies were plated onto LB agar plates selective for PA14 containing 100 µg/ml rifampicin (Sigma) and incubated overnight at 37°C. In total, bacterial colonies from three replicates per DGRP extreme line were counted.

Germ-free flies

Flies were transferred in empty bottles covered with a fruit juice agar plate (35×10 mm). The fruit juice agar plate was prepared following boiling of 2% agar dissolved in fruit juice and supplemented with Tegasept and propionic acid to final concentrations of 0.56% and 0.37%, respectively. Once the mixture was solidified, 0.2 ml of yeast paste (66% dry yeast dissolved in double-distilled H_2O) was transferred into the middle of each Petri dish. Flies were conditioned by feeding on fruit juice agar plates for a day before being transferred into clean bottles with freshly prepared fruit juice agar plates on the top. After a 15 h incubation at 25°C, the eggs were collected into a mesh basket using a brush. Each basket was placed in a beaker containing 20 ml of 50% bleach for a maximum of 2 min or until ∼80% of dorsal appendages were dissolved as a result of removal of the chorion layer. Bleached eggs were then washed with sterile double-distilled H_2O under the microbiological hood and transferred into bottles containing sterile fly food and maintained at 25°C. Once the offspring began to emerge, they were transferred into bottles with sterile food. Lysates obtained from the emerged flies were plated onto LB media and incubated at 37°C overnight to ensure that they were germ-free.

Drosophila aging experiments

Flies were maintained at 25°C on our standard yeast–cornmeal–sucrose food. *w/UAS-srcGFP; Dl-Gal4* and *OreR/UAS-srcGFP; Dl-Gal4* flies were produced by crossing *w; UAS-srcGFP/CyO; Dl-Gal4/TM6C* to w^{1118} and Oregon R. DGRP lines #28194 and #28217 with GFP-marked ISCs were produced by backcrossing *UAS-srcGFP/+; Dl-Gal4/+* flies to the original DGRP lines for six generations and selecting GFP+ larvae in each generation. Following mating for 4 days, males and females were kept separated, 20 flies per vial, and flipped on fresh food every 2 days for the first 20 days and then every day from day 20 to 42. ISC/EE clusters of 5, 6, 7 and ≥8 cells and anti-pH3 reactivity were measured from female flies stained with anti-GFP and either anti-Prospero or anti-pH3 at 4, 30 and 42 days. For tumor detection, male flies of one cohort per genotype were dissected at 42 days of age and stained with anti-GFP, anti-Prospero and DAPI for tumor assessment. Tumors were defined as masses of >100 cells that were GFP+ and/or Prospero+ and had smaller nuclei than mature ECs.

Acknowledgements

The authors thank Norbert Perrimon, Bruce Edgar, Steven Hou, the BDSC and the VDRC for fly stocks. Monoclonal antibodies were obtained from the Developmental Studies Hybridoma Bank.

Competing interests

The authors declare no competing or financial interests.

Author contributions

Conceptualization: C.P., Y.A.; Methodology: C.P., Y.A.; Formal analysis: V.T., M. Panagi, C.P.; Investigation: V.T., M. Panagi, A.T., M.D., M.M., M. Papadopoulou, S.T., C.P.; Writing - original draft: Y.A., C.P., M. Panagi; Writing - review & editing: Y.A., C.P.; Supervision: C.P., Y.A.; Project administration: C.P., Y.A.; Funding acquisition: C.P., Y.A.

Funding

This work was supported by Marie Curie Career Integration Grants to Y.A. and C.P.

Supplementary information

Supplementary information available online at
http://dev.biologists.org/lookup/doi/10.1242/dev.189472.supplemental

References

Agrawal, N., Delanoue, R., Mauri, A., Basco, D., Pasco, M., Thorens, B. and Léopold, P. (2016). The Drosophila TNF Eiger is an adipokine that acts on insulin-producing cells to mediate nutrient response. *Cell Metab.* **23**, 675-684. doi:10.1016/j.cmet.2016.03.003

Amcheslavsky, A., Jiang, J. and Ip, Y. T. (2009). Tissue damage-induced intestinal stem cell division in *Drosophila*. *Cell Stem Cell* **4**, 49-61. doi:10.1016/j.stem.2008.10.016

Andersen, D. S., Colombani, J., Palmerini, V., Chakrabandhu, K., Boone, E., Röthlisberger, M., Toggweiler, J., Basler, K., Mapelli, M., Hueber, A.-O. et al. (2015). The Drosophila TNF receptor grindelwald couples loss of cell polarity and neoplastic growth. *Nature* **522**, 482. doi:10.1038/nature14298

Apidianakis, Y. and Rahme, L. G. (2011). Drosophila Melanogaster as a model for human intestinal infection and pathology. *Dis. Model. Mech.* **4**, 21-30. doi:10.1242/dmm.003970

Apidianakis, Y., Pitsouli, C., Perrimon, N. and Rahme, L. (2009). Synergy between bacterial infection and genetic predisposition in intestinal dysplasia. *Proc. Natl. Acad. Sci. USA* **106**, 20883-20888. doi:10.1073/pnas.0911797106

Balkwill, F. and Mantovani, A. (2001). Inflammation and cancer: back to virchow? *Lancet* **357**, 539-545. doi:10.1016/S0140-6736(00)04046-0

Biteau, B., Hochmuth, C. E. and Jasper, H. (2008). JNK activity in somatic stem cells causes loss of tissue homeostasis in the aging *Drosophila* gut. *Cell Stem Cell* **3**, 442-455. doi:10.1016/j.stem.2008.07.024

Biteau, B., Karpac, J., Supoyo, S., DeGennaro, M., Lehmann, R. and Jasper, H. (2010). Lifespan extension by preserving proliferative homeostasis in Drosophila. *PLoS Genet.* **6**, e1001159. doi:10.1371/journal.pgen.1001159

Bortner, D. M. and Rosenberg, M. P. (1997). Induction of mammary gland hyperplasia and carcinomas in transgenic mice expressing human cyclin E. *Mol. Cell. Biol.* **17**, 453-459. doi:10.1128/MCB.17.1.453

Buchon, N., Broderick, N. A., Kuraishi, T. and Lemaitre, B. (2010). Drosophila EGFR pathway coordinates stem cell proliferation and gut remodeling following infection. *BMC Biol.* **8**, 152. doi:10.1186/1741-7007-8-152

Buchon, N., Osman, D., David, F. P. A., Yu Fang, H., Boquete, J.-P., Deplancke, B. and Lemaitre, B. (2013). Morphological and molecular characterization of adult midgut compartmentalization in Drosophila. *Cell Rep.* **3**, 1725-1738. doi:10.1016/j.celrep.2013.04.001

Chakrabarti, S., Dudzic, J. P., Li, X., Collas, E. J., Boquete, J.-P. and Lemaitre, B. (2016). Remote control of intestinal stem cell activity by haemocytes in Drosophila. *PLoS Genet.* **12**, e1006089. doi:10.1371/journal.pgen.1006089

Chatterjee, M. and Ip, Y. T. (2009). Pathogenic stimulation of intestinal stem cell response in Drosophila. *J. Cell. Physiol.* **220**, 664-671. doi:10.1002/jcp.21808

Chen, J., Xu, N., Huang, H., Cai, T. and Xi, R. (2016). A feedback amplification loop between stem cells and their progeny promotes tissue regeneration and tumorigenesis. *eLife* **5**, e14330. doi:10.7554/eLife.14330

Choi, N. H., Lucchetta, E. and Ohlstein, B. (2011). Nonautonomous regulation of Drosophila midgut stem cell proliferation by the insulin-signaling pathway. *Proc. Natl. Acad. Sci. USA* **108**, 18702-18707. doi:10.1073/pnas.1109348108

Denchi, E. L., Celli, G. and de Lange, T. (2006). Hepatocytes with extensive telomere deprotection and fusion remain viable and regenerate liver mass through endoreduplication. *Genes Dev.* **20**, 2648-2653. doi:10.1101/gad.1453606

Donnellan, R. and Chetty, R. (1999). Cyclin E in human cancers. *FASEB J.* **13**, 773-780. doi:10.1096/fasebj.13.8.773

Doupé, D. P., Marshall, O. J., Dayton, H., Brand, A. H. and Perrimon, N. (2018). Drosophila intestinal stem and progenitor cells are major sources and regulators of homeostatic niche signals. *Proc. Natl Acad. Sci. USA* **115**, 12218-12223. doi:10.1073/pnas.1719169115

Duronio, R. J. and O'Farrell, P. H. (1994). Developmental control of a G1-S transcriptional program in Drosophila. *Development* **120**, 1503-1515.

Dutta, D., Dobson, A. J., Houtz, P. L., Gläßer, C., Revah, J., Korzelius, J., Patel, P. H., Edgar, B. A. and Buchon, N. (2015). Regional cell-specific transcriptome mapping reveals regulatory complexity in the adult Drosophila midgut. *Cell Rep.* **12**, 346-358. doi:10.1016/j.celrep.2015.06.009

Evangelou, A., Ignatiou, A., Antoniou, C., Kalanidou, S., Chatzimatthaiou, S., Shianiou, G., Ellina, S., Athanasiou, R., Panagi, M., Apidianakis, Y. et al. (2019). Unpredictable effects of the genetic background of transgenic lines in physiological quantitative traits. *G3 (Bethesda).* **9**, 3877-3890. doi:10.1534/g3.119.400715

Fagerland, M. W. and Sandvik, L. (2009). Performance of five two-sample location tests for skewed distributions with unequal variances. *Contemp. Clin. Trials* **30**, 490-496. doi:10.1016/j.cct.2009.06.007

Ferrandon, D. (2013). The complementary facets of epithelial host defenses in the genetic model organism Drosophila melanogaster: from resistance to resilience. *Curr. Opin. Immunol.* **25**, 59-70. doi:10.1016/j.coi.2012.11.008

Go, M. J., Eastman, D. S. and Artavanis-Tsakonas, S. (1998). Cell proliferation control by Notch signaling in Drosophila development. *Development* **125**, 2031-2040.

Guo, Z. and Ohlstein, B. (2015). Bidirectional Notch signaling regulates Drosophila intestinal stem cell multipotency. *Science* **350**, aab0988. doi:10.1126/science.aab0988

Hanahan, D. and Weinberg, R. A. (2011). Hallmarks of cancer: the next generation. *Cell* **144**, 646-674. doi:10.1016/j.cell.2011.02.013

Huh, C.-G., Factor, V. M., Sanchez, A., Uchida, K., Conner, E. A. and Thorgeirsson, S. S. (2004). Hepatocyte growth factor/C-met signaling pathway is required for efficient liver regeneration and repair. *Proc. Natl. Acad. Sci. USA* **101**, 4477-4482. doi:10.1073/pnas.0306068101

Jiang, H., Patel, P. H., Kohlmaier, A., Grenley, M. O., McEwen, D. G. and Edgar, B. A. (2009). Cytokine/Jak/Stat signaling mediates regeneration and homeostasis in the Drosophila Midgut. *Cell* **137**, 1343-1355. doi:10.1016/j.cell.2009.05.014

Jiang, H., Grenley, M. O., Bravo, M.-J., Blumhagen, R. Z. and Edgar, B. A. (2011). EGFR/Ras/MAPK signaling mediates adult midgut epithelial homeostasis and regeneration in Drosophila. *Cell Stem Cell* **8**, 84-95. doi:10.1016/j.stem.2010.11.026

Karin, M. and Clevers, H. (2016). Reparative inflammation takes charge of tissue regeneration. *Nature* **529**, 307-315. doi:10.1038/nature17039

Klusza, S. and Deng, W.-M. (2011). At the crossroads of differentiation and proliferation: precise control of cell-cycle changes by multiple signaling pathways in Drosophila follicle cells. *BioEssays* **33**, 124-134. doi:10.1002/bies.201000089

Knoblich, J. A., Sauer, K., Jones, L., Richardson, H., Saint, R. and Lehner, C. F. (1994). Cyclin E controls S phase progression and its down-regulation during Drosophila embryogenesis is required for the arrest of cell proliferation. *Cell* **77**, 107-120. doi:10.1016/0092-8674(94)90239-9

Kondorosi, E., Roudier, F. and Gendreau, E. (2000). Plant cell-size control: growing by ploidy? *Curr. Opin. Plant Biol.* **3**, 488-492. doi:10.1016/S1369-5266(00)00118-7

Kux, K. and Pitsouli, C. (2014). Tissue communication in regenerative inflammatory signaling: lessons from the fly gut. *Front. Cell Infect. Microbiol.* **4**, 49. doi:10.3389/fcimb.2014.00049

Lasry, A., Zinger, A. and Ben-Neriah, Y. (2016). Inflammatory networks underlying colorectal cancer. *Nat. Immunol.* **17**, 230. doi:10.1038/ni.3384

Lee, K.-A., Kim, S.-H., Kim, E.-K., Ha, E.-M., You, H., Kim, B., Kim, M.-J., Kwon, Y., Ryu, J.-H. and Lee, W.-J. (2013). Bacterial-derived uracil as a modulator of mucosal immunity and gut-microbe homeostasis in *Drosophila*. *Cell* **153**, 797-811. doi:10.1016/j.cell.2013.04.009

Lee, K.-Z., Lestradet, M., Socha, C., Schirmeier, S., Schmitz, A., Spenlé, C., Lefebvre, O., Keime, C., Yamba, W. M., Aoun, R. B. et al. (2016). Enterocyte purge and rapid recovery is a resilience reaction of the gut epithelium to pore-forming toxin attack. *Cell Host Microbe* **20**, 716-730. doi:10.1016/j.chom.2016.10.010

Losick, V. P., Fox, D. T. and Spradling, A. C. (2013). Polyploidization and cell fusion contribute to wound healing in the adult Drosophila epithelium. *Curr. Biol.* **23**, 2224-2232. doi:10.1016/j.cub.2013.09.029

Mabery, E. M. and Schneider, D. S. (2010). The Drosophila TNF Ortholog Eiger is required in the fat body for a robust immune response. *J. Innate Immun.* **2**, 371-378. doi:10.1159/000315050

Mackay, T. F. C., Richards, S., Stone, E. A., Barbadilla, A., Ayroles, J. F., Zhu, D., Casillas, S., Han, Y., Magwire, M. M., Cridland, J. M. et al. (2012). The Drosophila melanogaster genetic reference panel. *Nature* **482**, 173. doi:10.1038/nature10811

Maeda, K., Takemura, M., Umemori, M. and Adachi-Yamada, T. (2008). E-cadherin prolongs the moment for interaction between intestinal stem cell and its progenitor cell to ensure Notch signaling in adult Drosophila Midgut. *Genes Cells* **13**, 1219-1227. doi:10.1111/j.1365-2443.2008.01239.x

Malumbres, M. and Barbacid, M. (2001). Milestones in cell division: to cycle or not to cycle: a critical decision in cancer. *Natu. Rev. Cancer* **1**, 222. doi:10.1038/35106065

Marianes, A. and Spradling, A. C. (2013). Physiological and stem cell compartmentalization within the Drosophila Midgut. *eLife* **2**, e00886. doi:10.7554/eLife.00886

Micchelli, C. A. and Perrimon, N. (2006). Evidence that stem cells reside in the adult Drosophila Midgut epithelium. *Nature* **439**, 475-479. doi:10.1038/nature04371

O'Brien, L. E., Soliman, S. S., Li, X. and Bilder, D. (2011). Altered modes of stem cell division drive adaptive intestinal growth. *Cell* **147**, 603-614. doi:10.1016/j.cell.2011.08.048

Ohlstein, B. and Spradling, A. (2006). The adult Drosophila posterior midgut is maintained by pluripotent stem cells. *Nature* **439**, 470-474. doi:10.1038/nature04333

Panayidou, S. and Apidianakis, Y. (2013). Regenerative inflammation: lessons from Drosophila intestinal epithelium in health and disease. *Pathogens* **2**, 209-231. doi:10.3390/pathogens2020209

Parisi, F., Stefanatos, R. K., Strathdee, K., Yu, Y. and Vidal, M. (2014). Transformed epithelia trigger non-tissue-autonomous tumor suppressor response by adipocytes via activation of toll and Eiger/TNF signaling. *Cell Rep.* **6**, 855-867. doi:10.1016/j.celrep.2014.01.039

Patel, P. H., Dutta, D. and Edgar, B. A. (2015). Niche appropriation by Drosophila intestinal stem cell tumours. *Nat. Cell Biol.* **17**, 1182-1192. doi:10.1038/ncb3214
Peterson, L. W. and Artis, D. (2014). Intestinal epithelial cells: regulators of barrier function and immune homeostasis. *Nat. Rev. Immunol.* **14**, 141. doi:10.1038/nri3608
Ranganayakulu, G., Schulz, R. A. and Olson, E. N. (1996). Wingless signaling induces nautilus expression in the ventral mesoderm of the Drosophila embryo. *Dev. Biol.* **176**, 143-148. doi:10.1006/dbio.1996.9987
Resende, L. P., Monteiro, A., Brás, R., Lopes, T. and Sunkel, C. E. (2018). Aneuploidy in intestinal stem cells promotes gut dysplasia in Drosophila. *J. Cell Biol.* **217**, 3930-3946. doi:10.1083/jcb.201804205
Sarov, M., Barz, C., Jambor, H., Hein, M. Y., Schmied, C., Suchold, D., Stender, B., Janosch, S., Kj, V. V., Krishnan, R. T. et al. (2016). A genome-wide resource for the analysis of protein localisation in Drosophila. *eLife* **5**, e12068. doi:10.7554/eLife.12068
Schneider, D. S. and Ayres, J. S. (2008). Two ways to survive infection: what resistance and tolerance can teach us about treating infectious diseases. *Nat. Rev. Immunol.* **8**, 889. doi:10.1038/nri2432
Shu, Z. and Deng, W.-M. (2017). Differential regulation of Cyclin E by Yorkie-scalloped signaling in organ development. *G3* **7**, 1049-1060. doi:10.1534/g3.117.039065
Shu, Z., Row, S. and Deng, W.-M. (2018). Endoreplication: the good, the bad, and the ugly. *Trends Cell Biol.* **28**, 465-474. doi:10.1016/j.tcb.2018.02.006
Siudeja, K., Nassari, S., Gervais, L., Skorski, P., Lameiras, S., Stolfa, D., Zande, M., Bernard, V., Frio, T. R. and Bardin, A. J. (2015). Frequent somatic mutation in adult intestinal stem cells drives neoplasia and genetic mosaicism during aging. *Cell Stem Cell* **17**, 663-674. doi:10.1016/j.stem.2015.09.016
Tamori, Y. and Deng, W.-M. (2013). Tissue repair through cell competition and compensatory cellular hypertrophy in postmitotic epithelia. *Dev. Cell* **25**, 350-363. doi:10.1016/j.devcel.2013.04.013
Tamori, Y. and Deng, W.-M. (2014). Compensatory cellular hypertrophy: the other strategy for tissue homeostasis. *Trends Cell Biol.* **24**, 230-237. doi:10.1016/j.tcb.2013.10.005
Taniguchi, K., Wu, L.-W., Grivennikov, S. I., de Jong, P. R., Lian, I., Yu, F.-X., Wang, K., Ho, S. B., Boland, B. S., Chang, J. T. et al. (2015). A gp130-Src-YAP module links inflammation to epithelial regeneration. *Nature* **519**, 57-62. doi:10.1038/nature14228
Tomasetti, C. and Vogelstein, B. (2015). Cancer Etiology. Variation in cancer risk among tissues can be explained by the number of stem cell divisions. *Science* **347**, 78-81. doi:10.1126/science.1260825
Tomasetti, C., Li, L. and Vogelstein, B. (2017). Stem cell divisions, somatic mutations, cancer etiology, and cancer prevention. *Science* **355**, 1330-1334. doi:10.1126/science.aaf9011
Webster, M., Witkin, K. L. and Cohen-Fix, O. (2009). Sizing up the nucleus: nuclear shape, size and nuclear-envelope assembly. *J. Cell Sci.* **122**, 1477-1486. doi:10.1242/jcs.037333
Weiss, A., Herzig, A., Jacobs, H. and Lehner, C. F. (1998). Continuous Cyclin E expression inhibits progression through endoreduplication cycles in Drosophila. *Curr. Biol.* **8**, 239-242. doi:10.1016/S0960-9822(98)70090-9
Wu, S., Powers, S., Zhu, W. and Hannun, Y. A. (2016). Substantial contribution of extrinsic risk factors to cancer development. *Nature* **529**, 43. doi:10.1038/nature16166
Xiang, J., Bandura, J., Zhang, P., Jin, Y., Reuter, H. and Edgar, B. A. (2017). EGFR-dependent TOR-independent endocycles support Drosophila gut epithelial regeneration. *Nat. Commun.* **8**, 15125. doi:10.1038/ncomms15125
Zeng, X. and Hou, S. X. (2015). Enteroendocrine cells are generated from stem cells through a distinct progenitor in the adult Drosophila posterior midgut. *Development* **142**, 644-653. doi:10.1242/dev.113357
Zeng, X., Chauhan, C. and Hou, S. X. (2010). Characterization of midgut stem cell- and enteroblast-specific Gal4 lines in Drosophila. *Genesis* **48**, 607-611. doi:10.1002/dvg.20661
Zhai, Z., Kondo, S., Ha, N., Boquete, J.-P., Brunner, M., Ueda, R. and Lemaitre, B. (2015). Accumulation of differentiating intestinal stem cell progenies drives tumorigenesis. *Nat. Commun.* **6**, 10219. doi:10.1038/ncomms10219